Impacts of water partitioning and polarity of organic compounds on secondary organic aerosol over Eastern China

Jingyi Li[1, 2], Haowen Zhang[2], Qi Ying[3,*], Zhijun Wu[4, 1], Yanli Zhang[5,6], Xinming Wang[5,6,7], Xinghua Li[8], Yele Sun[9], Min Hu[4, 1], Yuanhang Zhang[4, 1], Jianlin Hu[1, 2, *]

[1] Collaborative Innovation Center of Atmospheric Environment and Equipment Technology, Nanjing University of Information Science & Technology, Nanjing 210044, China

[2] Jiangsu Key Laboratory of Atmospheric Environment Monitoring and Pollution Control, School of Environmental Science and Engineering, Nanjing University of Information Science & Technology, Nanjing 210044, China

[3] Zachry Department of Civil and Environmental Engineering, Texas A&M University, College Station, Texas 77843-3136, USA

[4] State Key Joint Laboratory of Environmental Simulation and Pollution Control, College of Environmental Sciences and Engineering, Peking University, Beijing 100871, China

[5] State Key Laboratory of Organic Geochemistry and Guangdong Key Laboratory of Environmental Protection and Resources Utilization, Guangzhou Institute of Geochemistry, Chinese Academy of Sciences, Guangzhou 510640, China

[6] Center for Excellence in Regional Atmospheric Environment, Institute of Urban Environment, Chinese Academy of Sciences, Xiamen 361021, China

[7] University of Chinese Academy of Sciences, Beijing 100049, China

[8] School of Space & Environment, Beihang University, Beijing 100191, China

[9] State Key Laboratory of Atmospheric Boundary Layer Physics and Atmospheric Chemistry, Institute of Atmospheric Physics, Chinese Academy of Sciences, Beijing 100029, China

Corresponding authors:
Qi Ying, Email: qying@civil.tamu.edu
Jianlin Hu, Email: jianlinhu@nuist.edu.cn

Abstract

Secondary organic aerosol (SOA) is an important component of fine particular matter (PM$_{2.5}$). Most air quality models use an equilibrium partitioning method along with the saturation vapor pressure (SVP) of semi-volatile organic compounds (SVOCs) to predict SOA formation. However, the models typically assume that the organic particulate matter (OPM) is an ideal mixture and ignore the partitioning of water vapor to OPM. In this study, the Community Multi-scale Air Quality model (CMAQ) is updated to investigate the impacts of water vapor partitioning and non-ideality of the organic-water mixture on SOA formation during winter (January) and summer (July) of 2013 over eastern China. The updated model treats the partitioning of water vapor molecules into OPM and uses the UNIFAC model to estimate the activity coefficients of species in the organic-water mixture. The modified model can generally capture the observed surface organic carbon (OC) with a correlation coefficient R of 0.7, and the surface OA with the mean fractional bias (MFB) and mean fractional error (MFE) of -0.28 and 0.54, respectively. SOA concentration shows significant seasonal and spatial variations, with high concentrations in the North China Plain (NCP), Central China and Sichuan basin (SCB) regions during winter (up to 25 μg m^{-3}) and in the Yangtze River Delta (YRD) during summer (up to 16 μg m^{-3}). In winter, SOA decreases slightly in the updated model, with the monthly-averaged relative change of 10-20% in the highly concentrated areas, mainly due to organic-water interactions. The monthly-averaged concentration of SOA increases greatly in summer, by 20-50% at the surface and 30-60% in the whole column. The increase of SOA is mainly due to the increase in biogenic SOA in inland areas and anthropogenic SOA in coastal areas. As a result, the averaged aerosol optical depth (AOD) is increased by up to 10% and the cooling effect of aerosol radiative forcing (ARF) is enhanced by up to 15% over YRD in summer. The aerosol liquid water content associated with OPM (ALW$_{org}$) at the surface is relatively high in inland areas in winter and over the ocean in summer, with the monthly-averaged concentration of 0.5-3.0 and 5-7 μg m^{-3}, respectively. The hygroscopicity parameter (κ) of

57 OA based on the κ-Köhler theory is determined using the modeled ALW$_{org}$. The

58 correlation of κ with O：C ratio varies significantly across different cities and seasons.

59 Analysis of two representative cities, Jinan (in NCP) and Nanjing (in YRD), shows that the

60 impacts of water partitioning and non-ideality of the organic-water mixture on SOA are

61 sensitive to temperature, relative humidity (RH), and the SVP of SVOCs. The two

62 processes exhibit opposite impacts on SOA in eastern China. Water uptake increases SOA

63 by up to 80% in the organic phase, while including non-unity activity coefficients decreases

64 SOA by up to 50%. Our results indicate that both water partitioning into OPM and the

65 activity coefficients of the condensed organics should be considered in simulating SOA

66 formation from gas-particle partitioning, especially in hot and humid environments.

67 **Keywords**: SOA, non-ideality, water partitioning, hygroscopicity

68 **1 Introduction**

69 Secondary organic aerosol (SOA) is formed via a complex interaction of volatile organic

70 compounds (VOCs) with oxidants and primary particles emitted from anthropogenic and

71 biogenic sources in the atmosphere. As an important component of fine particular matter

72 (PM$_{2.5}$), SOA can cause severe air pollution in urban and suburban areas (Huang et al.,

73 2014) and exhibit adverse health effects (Atkinson et al., 2014). SOA also plays an

74 important role in new particle formation and particle growth that further contribute to the

75 enhancement of cloud condensation nuclei (CCN) (Wiedensohler et al., 2009; Ehn et al.,

76 2014). This will, in turn, impact the atmospheric aerosol burden, precipitation and water

77 circulation, solar radiation budget, and climate (Ramanathan et al., 2001). However, the

78 extents of those influences are not well understood so far, due to the high uncertainties

79 associated with the formation and physical and chemical properties of SOA (Shrivastava

80 et al., 2017). Large gaps still exist in SOA mass loading and properties between models

81 and observations (Gentner et al., 2017; Ervens et al., 2011; Hayes et al., 2015). Therefore,

82 it is crucial to explore and resolve this issue to improve our knowledge of the roles of SOA

83 in the environment, human health, and climate.

84   Gas-particle partitioning of semi-volatile and low-volatile organic compounds

85   (SVOCs and LVOCs) generated from VOC oxidation is an important pathway of SOA

86   formation. In most current chemical transport models (CTMs), this process is treated as an

87   equilibrium partitioning process that depends on the mass concentration of the organic

88   particulate matter (OPM), ambient temperature (T), the mean molecular weight of OPM,

89   and the volatility of condensed organics (Pankow, 1994). The formation of condensed

90   organic products is commonly represented by lumped surrogate SVOCs in a 2-product

91   model with volatilities and SVOC yields fitted to chamber experiments (Odum et al., 1996).

92   To better represent the volatility of primary organic aerosol (POA) and the multi-generation

93   oxidation of SVOCs to a wider range, Donahue et al. (2006) proposed the volatility basis

94   set (VBS) model in which the mass yields of SVOCs are fitted to a fixed number of

95   volatility bins (usually 0.01-10^5 μg m^{-3}). The VBS model has been adopted by several

96   CTMs (such as WRF-Chem, GEOS-Chem, etc.).

97   Although the models can capture the general trend of SOA evolution and mass

98   concentration to some extent (Li et al., 2017a; Bergström et al., 2012; Woody et al., 2016),

99   two key factors currently neglected in models may lead to biases: 1) the molecular

100   structures and interactions of functional groups (-OH, -C=O, -COOH, etc.) of condensed

101   organics (non-ideality); 2) partitioning of water vapor, the most abundant atmospheric

102   constituent besides O_2 and N_2, to OPM. The non-ideality alters the volatility of condensed

103   organics, and thus their contributions to the total SOA mass loading (Cappa et al., 2008).

104   Water partitioning into OPM can reduce the partial pressure of organics due to Raoult's

105   Law effect (Prisle et al., 2010) and lead to increases in SOA mass. The amount of aerosol

106   liquid water associated with organics (ALW$_{org}$) may vary for different precursors (Healy et

107   al., 2009; Prisle et al., 2010). The above two aspects will not only affect the chemical

108   composition of SOA but also the inorganic portion (Ansari and Pandis, 2000) and optical

109   properties (Denjean et al., 2015) of aerosols.

110   Laboratory and field studies have observed water absorbed by SOA from a variety of

111   precursor VOCs (Lambe et al., 2011; Zhao et al., 2016b; Asa-Awuku et al., 2010;

112   Varutbangkul et al., 2006). The hygroscopicity of SOA, quantitatively described by the

113   hygroscopicity parameter, κ, is correlated with the oxygen-to-carbon ratio (O:C) and

114   increases with more oxidized SOA during photochemical aging (Lambe et al., 2011;Zhao

115   et al., 2016b). The OPM-associated water can be estimated using the κ-Köhler theory under

116   the Zdanovskii-Stokes-Robinson (ZSR) assumption of no interactions between any

117   constitutes in aerosols (Petters and Kreidenweis, 2007). The total water content is the

118   summation of water associated with each solute at the same water activity. Guo et al. (2015)

119   found that this simplified method, along with the ISORROPIA model which is used to

120   predict aerosol liquid water (ALW) associated with the inorganic portion of aerosols, could

121   reproduce the observed total ALW in the ambient environment. Pye et al. (2017) found that

122   the modeled organic aerosol (OA) improved significantly but biased high at nighttime

123   when ALW_{org} is included in the calculation. However, as the interaction among organic

124   species and between organics and water in the organic-water mixture has been shown to

125   play an important role in SOA formation and water partitioning to OPM (Kim et al., 2019),

126   the ALW_{org} estimated by the κ-Köhler theory and its impact on SOA might not be accurate.

127   Using UNIversal Functional Activity Coefficient (UNIFAC) method (Fredenslund et al.,

128   1975) for calculating activity coefficients of the organic-water mixture, it was found that

129   in the eastern U.S., where biogenic SOA dominated the OA, considering ALW_{org} leads to

130   a significant increase in predicted SOA (Pankow et al., 2015; Jathar et al., 2016).

131   China has been suffering from severe $PM_{2.5}$ pollution especially in the eastern region

132   with fast urbanization and economic development (Fu and Chen, 2017). SOA is a very

133   important component of $PM_{2.5}$ in China that contributes about 20-50% (Li et al., 2017b).

134   The fraction of SOA in OA increases during haze events (Huang et al., 2014; Sun et al.,

135   2019). Previous modeling studies in China indicate that SOA was underpredicted (Lin et

136　al., 2016; Jiang et al., 2012) and the impacts of the non-ideality and water-OPM partitioning

137　on modeled SOA have not been evaluated.

138　　In this study, regional simulations of SOA during January and July of 2013 over

139　eastern China were conducted to investigate the seasonal variation of SOA due to water

140　partitioning into OPM. The model performance was evaluated against observed

141　meteorological parameters (temperature and relative humidity, RH) as well as $PM_{2.5}$,

142　organic carbon (OC), and OA at ground monitoring sites. The regional and seasonal

143　impacts on SOA, ALW_{org}, and properties of aerosols were quantified. Lastly, influences of

144　the results by several factors including meteorological parameters, estimations of saturation

145　vapor pressures (SVP) of condensed organics, and the individual impacts of ALW_{org} and

146　non-ideality of the organic-water mixture on SOA prediction were analyzed.

147　**2 Methodology**

148　**2.1 Model description**

149　The Community Multi-scale Air Quality model (CMAQ v5.0.1) coupled with a modified

150　SAPRC-11 was used in this study. Model configurations were largely based on that used

151　by Hu et al. (2016) as summarized below. Firstly, SAPRC-11 was expanded for a more

152　detailed treatment of isoprene oxidation and tracking dicarbonyl products (glyoxal and

153　methylglyoxal) from different groups of major precursors (Ying et al., 2015). Secondly,

154　SOA from isoprene epoxydiols (IEPOX), methacrylic acid epoxide (MAE) and dicarbonyls

155　through surface-controlled irreversible reactive uptake were added (Hu et al., 2017; Li et

156　al., 2015; Liu et al., 2020; Ying et al., 2015). Thirdly, the heterogeneous formation of

157　secondary nitrate and sulfate from NO_2 and SO_2 reaction on the particle surfaces (Ying et

158　al., 2014) were added, which is an important source of secondary inorganic aerosols (Zheng

159　et al., 2015) and improves model estimates of nitrate and sulfate (Qiao et al., 2018; Shi et

160　al., 2017). Fourthly, SOA yields were corrected for vapor wall loss (Zhang et al., 2014).

161　Impacts of the above updates on model performances have been extensively discussed in

162　the cited work and will not be further investigated in the current study.

163   The SOA module mostly follows Pankow et al. (2015). Two types of SOA as

164   traditionally treated in CMAQ were considered, "semi-volatile" (SV) portion that formed

165   via equilibrium absorption-partitioning of SVOCs, and "non-volatile" (NV) portion that

166   includes the oligomers and SOA formed via direct oxidation of aromatics at low-NO_x. SOA

167   from dicarbonyls, IEPOX, and MAE were formed by irreversible reactive uptake and

168   categorized as NV-SOA in the current model as well. Some studies investigated SOA from

169   glyoxal, methylglyoxal, and IEPOX using detailed reactions and reversible pathways in

170   models or observed as reversible processes in chamber experiments, leading to a relatively

171   lower SOA yield compared to the surface-controlled irreversible uptake (Lim et al., 2013;

172   Knote et al., 2014; Galloway et al., 2009; El-Sayed et al., 2018; Budisulistiorini et al., 2017).

173   The non-volatile assumption used in this paper allows an upper-limit estimation of the

174   importance of these additional SOA formation pathways. POA was treated as non-volatile

175   and non-reactive. The mass distribution of SVOCs between the gas-phase and particle-

176   phase follows the equation:

$$K_{p,i} = \frac{F_i}{M \cdot A_i} \tag{Eq1}$$

177   where $K_{p,i}$ $(m^3 \mu g^{-1})$ is the gas-particle partitioning constant for compound i, $F_i (\mu g \, m^{-3})$

178   is the concentration of species i in the particle-phase, A_i $(\mu g \, m^{-3})$ is the concentration of

179   species i in the gas-phase, and M $(\mu g \, m^{-3})$ is the total mass concentration of the absorbing

180   organic phase (i.e. OPM). The gas-particle partitioning constant $K_{p,i}$ is dependent on the

181   chemical composition of OPM. Pankow et al. (1994) derived $K_{p,i}$ for SVOCs partitioning

182   into an absorbing organic phase as:

$$K_{p,i} = \frac{RT}{10^6 \overline{MW} \xi_i p_{L,i}^o} \tag{Eq2}$$

183   where $p_{L,i}^o (atm)$ is the SVP of the pure compound i at temperature T(K), ξ_i is the activity

184   coefficient of species i in the absorbing organic phase, $\overline{MW}$ (g mol^{-1}) is the average

185   molecular weight of OPM, R (8.314 J mol^{-1} K^{-1}) is the gas constant, and 10^6 is used to

186   convert the units to $m^3 \mu g^{-1}$.

187   There are 12 lumped SVOCs generated by oxidation of alkanes, alkenes, and

188   aromatics under different NO_x conditions and 8 NV organic products as listed in Table S1

189   and Table S2. More details about the lumped precursors such as formation conditions

190   ("high" and "low" NO_x), lumping species and method, and yields from parent VOCs can

191   be found in Carlton et al. (2010) and summarized in SI. Activity coefficients of SVOCs

192   were calculated based on the composition of OPM using the UNIFAC method, with

193   assigned carbon number (n_c), functional groups and energy interaction parameters to both

194   SV and NV compounds (Pankow et al., 2015). The UNIFAC model is one of the commonly

195   used models that activity coefficients of condensed organics and their interactions with

196   water can be estimated. This method has been adopted to investigate the impacts of non-

197   ideality and water partitioning into OPM on SOA for different precursors in box models

198   (Seinfeld et al., 2001; Bowman and Melton, 2004) and CTMs (Pankow et al., 2015; Kim

199   et al., 2019). In the current model, POA was assumed to have a bulk composition of ten

200   categories of surrogate species (Table S3), as used by Li et al. (2015). POA is also involved

201   in the calculation of activity coefficients for the organic-water mixture. Detailed

202   information about the surrogate species including their structures and properties can be

203   found in Li et al. (2015) and references therein.

204   In addition to organic compounds, water partitioning into OPM is enabled according

205   to Eq 1 and Eq 2. In such a case, the absorbing phase in Eq 1 includes both organic aerosols

206   and water associated with OPM. As water condenses in the absorbing organic phase, it will

207   further alter the molar fraction of each composition, the activity coefficient of SVOCs and

208   the SV-SOA mass concentrations as a result. In the current model, we assumed no

209   interactions between the inorganic and organic phases.

210   **2.2 Estimating the hygroscopicity of OA**

211   Based on the κ-Köhler theory with linearly additive hygroscopic behavior of each

212   component of the mixed particle, ALW_{org} is related to the hygroscopicity parameter for the

213   organic mixture (κ_{org}) by Eq3 (Petters and Kreidenweis, 2007):

$$ALW_{org} = \rho_w V_{org} \kappa_{org} \frac{a_w}{1 - a_w} \qquad \text{(Eq3)}$$

214 where ρ_w is the density of water (assumed to be 1 g cm^{-1}), V_{org} is the volume concentration

215 of organics, and a_w is the water activity (assumed to be the same as RH). Since ALW$_{org}$

216 in this study is calculated mechanistically using the partitioning theory, κ_{org} can be

217 estimated by rearranging Eq3:

$$\kappa_{org} = \frac{ALW_{org}}{\rho_w V_{org}} \times \frac{1 - a_w}{a_w} \qquad \text{(Eq4)}$$

218 V_{org} can be estimated from the modeled mass concentration of OA, assuming the density

219 of OA to be 1.2 g cm^{-3} (Li et al., 2019).

220   In many studies, κ_{org} is assumed to increase linearly with the oxidation state of OA,

221 expressed as the O:C ratio (Massoli et al., 2010;Duplissy et al., 2011;Lambe et al., 2011).

222 The correlation of κ_{org} and O:C ratio at 9 representative cities was evaluated during

223 January and July of 2013, with the reduced major axis regression method (Ayers, 2001).

224 The O:C ratio was calculated using Eq5:

$$O:C = \sum_{i=1}^{n} f_i (O:C)_i \qquad \text{(Eq5)}$$

225 where f_i and $(O:C)_i$ are the molar fraction and O:C ratio of organic aerosol component

226 i. For POA, a fixed molar fraction and composition were assumed following Li et al. (2015).

227 For SOA, the O:C ratio was calculated by using their organic matter to organic carbon ratio

228 (OM:OC) following Simon and Bhave (2012):

$$O:C = \frac{12}{15} (OM:OC) - \frac{14}{15} \qquad \text{(Eq6)}$$

229 The OM:OC ratio of each SOA component follows Pankow et al. (2015) as shown in Table

230 S1-S2.

231 **2.3 Model application**

232 The simulation domain has a horizontal resolution of 36 km $\times$ 36 km (100 $\times$ 100 grids)

233 and a vertical structure of 18 layers up to 21 km, which covers eastern China as shown in

234 Figure S1. Anthropogenic emissions were generated from the Multi-resolution Emission

235 Inventory for China (MEIC) (Zhang et al., 2009) v1.0 with a 0.25°× 0.25° resolution

236 (http://www.meicmodel.org) for China, and the Regional Emission inventory in Asia

237 version 2 (REAS2) (Kurokawa et al., 2013) with a 0.25° × 0.25° resolution

238 (http://www.nies.go.jp/REAS/) for the rest of the domain. Biogenic emissions were

239 generated by the Model for Emissions of Gases and Aerosols from Nature (MEGAN) v2.1,

240 with the leaf area index (LAI) from the 8-day Moderate Resolution Imaging

241 Spectroradiometer (MODIS) LAI product (MOD15A2) and the plant function types (PFTs)

242 from the Global Community Land Model (CLM 3.0). Open biomass burning emissions

243 were generated from the Fire INvnetory from NCAR (FINN) (Wiedinmyer et al., 2011).

244 Dust and sea salt emissions were generated online during CMAQ simulations. The total

245 emissions of major SOA precursors and their spatial distributions are shown in Table S4

246 and Figure S2. Meteorological fields were generated using the Weather Research and

247 Forecasting (WRF) model v3.6.1 with initial and boundary conditions from the NCEP FNL

248 Operational Model Global Tropospheric Analyses dataset. More details about the model

249 application can be found in Hu et al. (2016).

250 Four scenarios are investigated in this study. The base case (BS) applies the default

251 secondary organic aerosol module of CMAQ v5.0.1. In this case, no water partitioning into

252 OPM is considered. Lumped semi-volatile products from the oxidation of various

253 precursors partition into a single organic phase, which is considered as an ideal mixture of

254 POA and SOA with γ_{org}=1. The water case (S1) includes water partitioning into OPM,

255 which is again considered as an ideal solution (γ_{org}=1 and $\gamma_{H2o} = 1$). The UNIFAC case

256 (S2) considers the interaction between organic constituents with UNIFAC calculated

257 activity coefficients ($\gamma_{org} \neq 1$) but does not allow water partitioning into OPM. The

258 combined case (S3) allows both water partitioning and interactions between all constituents

259 (including water and organics) using UNIFAC calculated activity coefficients ($\gamma_{org} \neq 1$

260 and $\gamma_{H2o} \neq 1$). The results of BS and S3 are used to examine the overall impacts of water

261 partitioning into OPM and polarity of organics on SOA and ALW_org, as shown in Section

262 3.1-3.4. The separate influences of those two processes on SOA from S1 and S2 are

263 discussed in Section 3.5.

264 **3 Results and discussion**

265 **3.1 Model evaluation**

266 The meteorological inputs and emissions have been used in several previous publications.

267 Model performance on meteorological parameters (temperature and RH), gaseous species

268 and gas and aerosol concentrations have been extensively evaluated (Hu et al., 2016; Hu et

269 al., 2017; Qiao et al., 2018; Shi et al., 2017). A summary of the model performance related

270 to this study is provided below. Observed meteorological data were obtained from the

271 National Climatic Data Center (ftp://ftp.ncdc.noaa.gov/pub/data/noaa). Observations of

272 OC at two urban locations, Beijing (Cao et al., 2014; Wang et al., 2015) and Guangzhou

273 (Lai et al., 2016) and OA in Beijing (Sun et al., 2014) during January of 2013 as well as

274 surface $PM_{2.5}$ at several monitoring sites during July of 2013 from China National

275 Environmental Monitoring Center (http://113.108.142.147:20035/emcpublish/) were used

276 to evaluate model estimates of aerosols. Details of measurement methodology and

277 uncertainties of observations are listed in the corresponding references.

278   Temperature and RH are the two meteorological factors that affect SOA formation.

279 Table 1 lists model statistics of mean observation (OBS), mean prediction (PRE), mean

280 bias (MB), gross error (GE) and correlation coefficient (R) based on WRF and observations

281 at monitoring sites located in 8 sub-regions of the domain (Figure S1) during January and

282 July of 2013. The benchmarks for the MM5 model (another meteorology model) of 4-12km

283 horizontal resolution suggested by Emery et al. (2001) are also listed in the table. Details

284 of monitoring sites in the 8 sub-regions are listed in Table S5. Overall, WRF tends to

285 underestimate both temperature and RH. The model shows better agreement with observed

286 temperature as R is higher than that of RH. Both temperature and RH are well captured by

287 the model in YRD, the Pearl River Delta (PRD), and the central regions of China (the major

288   regions of eastern China). In these regions, MB and GE of temperature are -1.2~0.7 K and

289   1.8~2.6 K, respectively, which are -11.8~5.6% and 9.2~16.8% for RH, respectively.

290   Model estimates of daily organic carbon (OC) from case S3 are compared with

291   measurements at monitoring sites in Beijing and Guangzhou in January of 2013 (Figure

292   1a). The factors used to convert SOA to OC (SOC) are listed in Table S1-S2. OC from

293   POA (POC) is directly predicted by the model. Generally, the ratio between modeled and

294   observed OC concentration falls in the range of 1:2 to 2:1, with an R-value of 0.7. The

295   model tends to underestimate OC on high concentration days. Overall, the mean fractional

296   bias (MFB) and mean fractional error (MFE) of OC are -0.20 and 0.27, within the criteria

297   (MFB≤ ±0.6; MFE≤0.75) suggested by EPA (2007). The bias in OC might be due to

298   underestimated POA emissions and underpredicted SOA in CMAQ from missing

299   precursors (Hu et al., 2017; Zhao et al., 2016a). No significant differences in OC are

300   observed in S3 compared to BS (not shown), likely due to the biased-low SOA predicted

301   in the current model that limits the impact of ALW_{org} on SOA formation.

302   The underestimate of SOA can be seen from Figure 1b as well. CMAQ can well

303   capture the observed diurnal variation of OA in Beijing during wintertime, except for the

304   underestimates of peak values. The correlation coefficient of modeled to observed OA is

305   0.55. We find a 25% underestimate of OA on average. Better agreement between the model

306   and observations is shown on non-polluted days (daily-averaged concentration less than 75

307    $\mu g\,m^{-3}$). The mean fractional bias (MFB) and mean fractional error (MFE) of polluted days

308   are -0.38 and 0.64, respectively, which are worse than that of the non-polluted days (-0.26

309   for MFB and 0.52 for MFE). The overall MFB and MFE of OA during January are -0.28

310   and 0.54, within the criteria (MFB≤ ±0.6; MFE≤0.75) suggested by EPA (2007). Again,

311   no apparent changes of SOA nor OA are observed between case S3 and BS (not shown),

312   since POA is predicted to be the primary contributor to OA at Beijing in winter in the

313   current model, with an averaged SOA/POA ratio of 0.12. This ratio is much lower than the

314   field observation of about 0.45-1.94 (Zhao et al., 2019; Sun et al., 2013; Sun et al., 2016).

315 The bias might be due to the missing SOA converted by partitioning and aging of semi-

316 volatile POA as well as oxidation from intermediate volatile organic compounds (IVOCs)

317 and VOC oxidation products. Those pathways are shown to be important for SOA

318 formation by modeling, field and chamber studies (Hodzic et al., 2010; Jimenez et al., 2009;

319 Murphy et al., 2017; Robinson et al., 2007; Shrivastava et al., 2008; Tkacik et al., 2012;

320 Zhao et al., 2014; Zhao et al., 2016a).

321 A sensitivity test was performed by using the newest CMAQ model version 5.3.1 that

322 includes all the above processes in the aerosol module. The SOA/POA ratio in Beijing is

323 improved greatly to be 0.83 in winter. However, high uncertainties still exist in the

324 emissions of the involved precursors and characterization of SOA formation through these

325 processes, needing further constrains by observations. Their influences on water

326 partitioning into OPM and non-ideality of the organic-water mixture on SOA will be

327 evaluated in a future study.

328 Due to the lack of observed OC and OA in July of 2013, as an alternative, model

329 performances are evaluated by comparing predicted and observed $PM_{2.5}$ at ground sites

330 (Figure S1) as shown in Figure S3. Generally, the model can well reproduce the diurnal

331 variation of $PM_{2.5}$ in most regions. Predicted $PM_{2.5}$ on highly concentrated days is biased

332 low, especially in the North China Plain (NCP). NCP has the highest $PM_{2.5}$ ranging from

333 60 $\mu g\ m^{-3}$ to 300 $\mu g\ m^{-3}$. The bias in modeled $PM_{2.5}$ is significant in cities in Northwest.

334 This might be due to missing dust emissions in the current inventory (Hu et al., 2016). To

335 further evaluate the model performance, averaged MFB and MFE of modeled $PM_{2.5}$ are

336 plotted against observations of each site as shown in Figure S4. The criteria of MFB and

337 MFE followed recommendations by Boylan and Russell (2006). Our model performs well

338 since most of the predictions meet the criteria and a large fraction (>58%) meet the goal.

339 The averaged MFB and MFE across all the sites are -0.28 and 0.39, indicating slightly

340 underestimate of $PM_{2.5}$ by the model.

341 **3.2 Impacts on SOA and ALW$_{org}$**

342   The spatial distribution of SOA varies greatly in the two seasons. In winter, SOA is

343   relatively high in eastern SCB and the central and eastern provinces of Shandong, Henan,

344   Anhui, and Hubei (Figure 2 and Figure S5). Monthly-averaged SOA concentrations in the

345   above areas are up to 25 and 15-20 μg m^{-3}, respectively. Anthropogenic emissions are the

346   major sources of SOA (Figure S6), such as dicarbonyl products from the oxidation of

347   xylene and toluene (Hu et al., 2017). In summer, surface SOA is high in Northeast, NCP,

348   and YRD. The highest SOA occurs in Shanghai and Jiangsu provinces as well as the coastal

349   area of the Yellow Sea, with the value of ~9-16 μg m^{-3} at the surface and ~20-25 mg m^{-2} in

350   the column (col-SOA) of the atmosphere below 21 km (Figure S5). Different from winter

351   SOA, a significant fraction of summer SOA is originated from biogenic emissions (Figure

352   S7). Anthropogenic SOA is highly concentrated in the coastal areas of the Yellow Sea and

353   Bohai Bay.

354   Combined effects of water partitioning into OPM and non-ideality on SOA formation

355   also exhibit strong seasonal variation. In winter, SOA is slightly decreased by 1.5 μg m^{-3}

356   (10-20%) on average at the surface (Figure 2) and less than ~1 mg m^{-2} (20%) in the column

357   (Figure S5) over high SOA regions where anthropogenic sources dominate. We show later

358   that the decrease of SOA is mainly due to the large activity coefficients of SVOCs which

359   decrease $K_{p,i}$. In summer, higher temperature and RH promote water partitioning and SOA

360   formation so that SOA increases apparently over the entire domain, with the highest

361   enhancement of 2-4 μg m^{-3} (20-50%) at the surface (Figure 2) and 4-6 mg m^{-2} (30-60%) in

362   the column (Figure S5) over YRD and the coastal area of Yellow Sea. Anthropogenic SOA

363   dominates the total change in winter as shown in Figure S6. In summer, the increase of

364   SOA is attributed to biogenic sources in inland areas and anthropogenic sources over the

365   ocean (Figure S7).

366   Regional distribution of ALW$_{org}$ is similar to the change of SOA as shown in Figure

367   3. In winter, a maximum averaged concentration of 3.0 μg m^{-3} for ALW$_{org}$ occurs in the

368   high SOA region, where significant changes of SOA also occur. In other areas, the averaged

369 concentration of ALW$_{org}$ is about 0.5-1.5 μg m^{-3}. Overall, the average ratio of ALW$_{org}$ to

370 SOA is about 0.1-0.3 in winter. In summer, water partitioning into OPM mostly occurs in

371 the east coastal area at the surface where a significant increase of anthropogenic SOA (such

372 as those from toluene and xylenes) is observed. This might be due to the high polarity of

373 anthropogenic SVOCs (having more -COOH groups) that absorb more water. In the coastal

374 area, the averaged concentration of ALW$_{org}$ is about 5-7 μg m^{-3}, with the ALW$_{org}$ /SOA

375 ratio of 0.5-1.0. Over the land, the averaged concentration of ALW$_{org}$ is about 1-3 μg m^{-3}

376 (ALW$_{org}$/SOA ratio of 0.2-0.5) in Northeast and East China. Water partitioning is mostly

377 associated with biogenic SOA originated from isoprene and monoterpenes oxidation that

378 produces SVOCs with abundant OH group.

379   Based on the column concentrations of ALW$_{org}$ and ALW$_{org}$/SOA ratio (Figure S8),

380 in winter, more ALW$_{org}$ must have occurred in the south and southwest regions at higher

381 levels where a significant increase of col-SOA occurs (Figure S5). The averaged col-

382 ALW$_{org}$/col-SOA ratio in the high SOA area is 0.1-0.3. In summer, the ALW$_{org}$ must be

383 high at higher altitudes over the central regions in China. The maximum col-ALW$_{org}$ is

384 about 7 mg m^{-2} over YRD, with the col-ALW$_{org}$/col-SOA ratio of about 0.3.

385 **3.3 Impacts on aerosol properties**

386 Since ALW$_{org}$ is determined in S3, the values of κ_{org} can be estimated from the modeled

387 ALW$_{org}$, OA and RH using Eq 4. 9 representative cities were selected to investigate the

388 relationship of κ_{org} vs. O:C and its seasonal variation as shown in Figure S9 and S10.

389 The results of all the cities in winter and summer are merged and analyzed as shown in

390 Figure 4. Pairs of κ_{org} and O:C data are grouped into 10 O:C bins and the averaged κ_{org}

391 in each bin are then calculated. Overall, the estimated O:C ratio is within the range of 0.2-

392 0.8. The averaged κ_{org} in each O:C bin is less than 0.1 in winter, with the highest value

393 in Guangzhou. As more ALW$_{org}$ is formed in summer, the averaged κ_{org} also increases

394 greatly with the highest value of 0.35 in Beijing. The linear correlation between κ_{org} and

395 O:C shows significant spatial and seasonal variations. For example, the slope of κ_{org}-O:C

396   is 70-90% smaller in winter than in summer in the Northern cities such as Shenyang,

397   Beijing, Zhengzhou, and Xi'an. However, in Guangzhou, the slope is 83% higher in winter

398   than in summer. In Chengdu, the slope is quite similar in both seasons. Overall, the slope

399   of κ_{org} vs. O:C in the 9 cities is 0.16 in winter and 0.40 in summer. Most of the fitted

400   linear correlations of the individual city fall outside of the range of 0.18 to 0.37 suggested

401   in previous studies (Duplissy et al., 2011;Lambe et al., 2011;Massoli et al., 2010;Chang et

402   al., 2010), indicating that the hygroscopicity of organic aerosols cannot be simply

403   represented by a single parameter such as the O:C ratio (Rickards et al., 2013). In both

404   seasons, κ_{org} approaches zero and negative values as O:C decreases, which might be due

405   to the linear regression of κ_{org} and O:C. To avoid this, an exponential fitting of the two

406   variables is performed so that κ_{org} falls in the range of (0,1) and is positively correlated

407   with O:C. In this case, the fitted correlations are κ_{org}=1-exp(-(O:C/1.88)$^{2.29}$) and κ_{org}=1-

408   exp(-(O:C/1.06)$^{4.50}$) for January and July of 2013, respectively.

409   The impacts on aerosol optical depth (AOD) and aerosol radiative forcing (ARF) are

410   further investigated. Figure 5 shows the monthly-averaged AOD at 550 nm in January and

411   July of 2013. It is calculated by summarizing the product of model estimated extinction

412   coefficient of fine particles ($b_{ext,i}$) multiplied by the thickness (HL_i) in each layer:

$$AOD = \sum_{i=1}^{N} b_{ext,i} \times HL_i \qquad \text{(Eq6)}$$

413   where N is the number of layers. There are two methods to estimate the aerosol extinction

414   coefficient in CMAQv5.0.1. One is based on the Mie theory and the predicted aerosol

415   component concentrations ($b_{ext,m}$), and the other is based on correlation from the IMPROVE

416   monitoring network that considers the impacts of hygroscopicity of different aerosol

417   components ($b_{ext,r}$) (Malm et al., 1994). AOD calculated with the two types of extinction

418   coefficient are denoted as AOD$_m$ and AOD$_r$, respectively.

419   In Figure 5, a clear pattern of high AOD$_r$ in SCB and NCP and low AOD$_r$ in west

420   China is observed in both winter and summer, consistent with previous studies (He et al.,

421 2019; He et al., 2016; Luo et al., 2014). An identical trend in AOD_m is shown in Figure

422 S11. The monthly-averaged AOD_r ranges from 1.0 to 3.2 in January and from 0.3 to 0.9 in

423 July. AOD_m is lower than AOD_r, falling in 0.7-2.2 in January and 0.3-0.6 in July. The

424 model significantly overestimates AOD in January but agrees better with observations from

425 MODIS where AOD is high in July (Figure S12). The bias in the predicted AOD might be

426 partially due to the empirical equation applied in the calculation of AOD in CMAQ (Wang

427 et al., 2009; Liu et al., 2010), and partially due to the uncertainties of fine AOD overland

428 from MODIS data (Wang et al., 2009; Levy et al., 2010). The increase of AOD due to

429 ALW_{org} shows a strong spatial and seasonal pattern. In winter, there are no significant

430 changes in AOD_r across the whole domain, due to insignificant changes of SOA. In summer,

431 AOD_r increases significantly in YRD and the adjacent areas by up to 10%.

432 　　ARF represents the change in the radiative flux at the top of the atmosphere due to

433 aerosols. An offline version of the Shortwave Radiative Transfer Model For GCMs

434 (RRTMG_SW) was used to calculate the direct radiative effect of aerosols on shortwave

435 radiation (Iacono et al., 2008). Generally, fine aerosols exhibit cooling effects on the

436 shortwave radiation in both winter and summer over the entire domain as shown in Figure

437 6. This impact is much stronger in the areas where AOD is high (Figure 5). The ARF is

438 highest in Shandong in winter and in the coastal area near Jiangsu province in summer,

439 which are about -5 W m^{-2} and -6 W m^{-2}, respectively. In winter, no significant changes of

440 ARF are observed in eastern China (Figure 6b). This is likely attributed to an insignificant

441 contribution of SOA to $PM_{2.5}$ in winter compared to other components with cooling effects,

442 such as sulfate. In summer, SOA is an important component of $PM_{2.5}$ (20-60%), and the

443 effects of water partitioning on shortwave radiation are relatively stronger. An

444 enhancement of up to 15% in the cooling effects of ARF occurs near the YRD region where

445 AOD significantly changes as well.

446 **3.4 Sensitivity to T, RH, and SVP**

447   Meteorological conditions and SOA precursors affect the impacts of water partitioning on

448   SOA. To better illustrate the dependency of SOA on temperature, RH, and SVP of SVOCs,

449   an offline calculation of SOA formation was performed at two representative cities (Jinan

450   in NCP during winter and Nanjing in YRD during summer) when the daily maximum SOA

451   increases occurred. We assume temperature (T) and water vapor mixing ratio (QV) to be

452   within the range of $\bar{X} \pm \sigma$, where $\bar{X}$ and σ are the mean and standard deviation

453   calculated based on WRF predictions at each location. We choose 10 evenly distributed

454   values for T and QV within the range of $\bar{X} \pm \sigma$. The temperature dependence parameter of

455   SVP ($\Delta H/R$) is also scaled by 0.2, 0,8, 1.4, and 2.0 separately for all the SVOCs. As shown

456   in Figure 7, SOA exhibits a negative correlation with T and a positive correlation with QV

457   in both cities. SOA is more sensitive to QV under cold conditions (Jinan) and to

458   temperature under hot conditions (Nanjing). When the temperature is fixed, the sensitivity

459   of SOA to $\Delta H/R$ is different in the two cities. We find more changes in SOA across $\Delta H/R$

460   in Jinan. This is attributed to the temperature correction factor (ζ_{corr}) of K_p in CMAQ as

461   defined below:

$$\zeta_{corr} = \frac{K_{p,T_{ref}}}{K_{p,T}} = \frac{T_{ref}}{T} \exp\left[\frac{\Delta H}{R}\left(\frac{1}{T_{ref}} - \frac{1}{T}\right)\right] \qquad (Eq8)$$

462   where T_{ref} is the reference temperature (298K) and T is temperature. According to

463   Figure 7, the range of T is 265-274K in Jinan and 300-307K in Nanjing. The deviation of

464   temperature from the reference value (298K) is greater in Jinan than in Nanjing. Therefore,

465   the unit change of $\Delta H/R$ causes greater variations of ζ_{corr} and thus K_p in Jinan. As a

466   result, SOA is more sensitive to $\Delta H/R$. The impacts of SVP estimation on SOA are more

467   significant in winter than in summer.

468   **3.5 Separate impacts of water partitioning/polarity of condensed organics**

469   Impacts of water partitioning into OPM and non-ideality of the organic-water mixture on

470   SOA are in opposite directions. Water partitioning increases SOA by ~10-20% in winter

471   and ~30-80% in summer in most areas of the domain (Figure 8). This is because the

472   molecular weight of water is quite small and will reduce the molar averaged weight of

473   OPM ($\overline{MW}$) in Eq2 (Pankow et al., 2015). The reduced $\overline{MW}$ further increases K_p and

474   promotes mass transfer of SVOCs from the gas-phase to OPM. On the other hand, by

475   considering non-ideality of the organic-water mixture, activity coefficients of SVOCs are

476   usually greater than 1.0 in this study, leading to a decrease in K_p. As a result, the total SOA

477   concentration is reduced by ~10-20% in winter and ~10-50% in summer (Figure 9). Overall,

478   the final impacts are the combined consequences of the two processes. In winter, the

479   increase of SOA caused by water partitioning is offset by the decrease of SOA due to the

480   polarity of SVOCs in most areas of the domain, resulting in slight decreases of SOA. In

481   summer, the effect of water partitioning overcomes that of SVOC polarity so the total SOA

482   loading increases. This further leads to an enhanced attenuation of shortwave solar

483   radiation and cooling of the atmosphere.

484   **4 Conclusions**

485   The WRF/CMAQ model was used to investigate the impacts of water partitioning into

486   OPM and non-ideality of the organic-water mixture on SOA formation over eastern China

487   during January and July of 2013. SOA is greatly enhanced in summer especially in YRD

488   and over the Yellow Sea by up to 50% and 60% at the surface and in the whole column,

489   respectively. No significant impacts on SOA are observed in winter. This might be due to

490   the underestimation of SOA in the current model. ALW$_{org}$ is highly correlated with the

491   change of SOA, with the ratio of ALW$_{org}$ to SOA of 0.1-0.3 and 0.2-1.0 at the surface

492   where significant changes of SOA occur in winter and summer, respectively. By using the

493   modeled ALW$_{org}$, correlations between κ_{org} and O:C are examined in 9 representative

494   cities, showing significant spatial and seasonal variations. The increases in SOA lead to an

495   enhancement in the averaged AOD and the cooling effects of aerosols, by up to 10% and

496   15% respectively in summer. The model predicted SOA is sensitive to temperature and QV

497   in both seasons, with higher sensitivity to QV during winter and temperature during

498   summer. Estimation of SVP also affects modeled SOA, especially in a cold environment.

499 The effects of water partitioning into OPM and non-ideality of the organic-water mixture

500 on SOA are the opposite. Since the activity coefficients of SVOCs are mostly greater than

501 1.0 during the simulated episode, SOA concentration decreases when the non-ideality

502 effect is considered. Averaged SOA concentration decreases by up to 20% in winter and

503 50% in summer. Water partitioning alone increases SOA by 10-20% in winter and 30-80%

504 in summer. It should be noticed that the results shown in this study are the lower limit as

505 the current model tends to underestimate SOA. It is crucial to consider both effects in

506 simulating SOA formation under hot and humid conditions in CTMs.

507

508 **Data availability**

509 Data used in this manuscript can be provided upon request by e-mail to the corresponding
510 authors, Qi Ying (qying@civil.tamu.edu) and Jianlin Hu (jianlinhu@nuist.edu.cn).

511

512 **Competing interests**
513 The authors declare that they have no conflict of interest.

514

523

524 **References**
525 Ansari, A. S., and Pandis, S. N.: Water Absorption by Secondary Organic Aerosol and Its
526 Effect on Inorganic Aerosol Behavior, Environ. Sci. Technol.,, 34, 71-77,
527 10.1021/es990717q, 2000.
528 Asa-Awuku, A., Nenes, A., Gao, S., Flagan, R. C., and Seinfeld, J. H.: Water-soluble SOA
529 from Alkene ozonolysis: composition and droplet activation kinetics inferences from

analysis of CCN activity, Atmos. Chem. Phys., 10, 1585-1597, 10.5194/acp-10-1585-2010, 2010.

Atkinson, R. W., Kang, S., Anderson, H. R., Mills, I. C., and Walton, H. A.: Epidemiological time series studies of PM2.5 and daily mortality and hospital admissions: a systematic review and meta-analysis, Thorax, 69, 660-665, 10.1136/thoraxjnl-2013-204492 %J Thorax, 2014.

Ayers, G. P.: Comment on regression analysis of air quality data, Atmos. Environ., 35, 2423-2425, https://doi.org/10.1016/S1352-2310(00)00527-6, 2001.

Bergström, R., Denier van der Gon, H. A. C., Prévôt, A. S. H., Yttri, K. E., and Simpson, D.: Modelling of organic aerosols over Europe (2002-2007) using a volatility basis set (VBS) framework: application of different assumptions regarding the formation of secondary organic aerosol, Atmos. Chem. Phys., 12, 8499-8527, 10.5194/acp-12-8499-2012, 2012.

Bowman, F. M., and Melton, J. A.: Effect of activity coefficient models on predictions of secondary organic aerosol partitioning, J. Aerosol Sci., 35, 1415-1438, https://doi.org/10.1016/j.jaerosci.2004.07.001, 2004.

Boylan, J. W., and Russell, A. G.: PM and light extinction model performance metrics, goals, and criteria for three-dimensional air quality models, Atmos. Environ., 40, 4946-4959, https://doi.org/10.1016/j.atmosenv.2005.09.087, 2006.

Budisulistiorini, S. H., Nenes, A., Carlton, A. G., Surratt, J. D., McNeill, V. F., and Pye, H. O. T.: Simulating Aqueous-Phase Isoprene-Epoxydiol (IEPOX) Secondary Organic Aerosol Production During the 2013 Southern Oxidant and Aerosol Study (SOAS), Environ. Sci. Technol.,, 51, 5026-5034, 10.1021/acs.est.6b05750, 2017.

Cappa, C. D., Lovejoy, E. R., and Ravishankara, A. R.: Evidence for liquid-like and nonideal behavior of a mixture of organic aerosol components, P. Natl. Acad. Sci. USA, 105, 18687-18691, 10.1073/pnas.0802144105, 2008.

Carlton, A. G., Bhave, P. V., Napelenok, S. L., Edney, E. O., Sarwar, G., Pinder, R. W., Pouliot, G. A., and Houyoux, M.: Model Representation of Secondary Organic Aerosol in CMAQv4.7, Environ. Sci. Technol.,, 44, 8553-8560, 10.1021/es100636q, 2010.

Chang, R. Y. W., Slowik, J. G., Shantz, N. C., Vlasenko, A., Liggio, J., Sjostedt, S. J., Leaitch, W. R., and Abbatt, J. P. D.: The hygroscopicity parameter (κ) of ambient organic aerosol at a field site subject to biogenic and anthropogenic influences: relationship to degree of aerosol oxidation, Atmos. Chem. Phys., 10, 5047-5064, 10.5194/acp-10-5047-2010, 2010.

Denjean, C., Formenti, P., Picquet-Varrault, B., Pangui, E., Zapf, P., Katrib, Y., Giorio, C., Tapparo, A., Monod, A., Temime-Roussel, B., Decorse, P., Mangeney, C., and Doussin, J. F.: Relating hygroscopicity and optical properties to chemical composition and structure of secondary organic aerosol particles generated from the ozonolysis of α-pinene, Atmos. Chem. Phys., 15, 3339-3358, 10.5194/acp-15-3339-2015, 2015.

Donahue, N. M., Robinson, A. L., Stanier, C. O., and Pandis, S. N.: Coupled partitioning, dilution, and chemical aging of semivolatile organics, Environ. Sci. Technol.,, 40, 02635-

02643, 10.1021/es052297c, 2006.

Duplissy, J., DeCarlo, P. F., Dommen, J., Alfarra, M. R., Metzger, A., Barmpadimos, I., Prevot, A. S. H., Weingartner, E., Tritscher, T., Gysel, M., Aiken, A. C., Jimenez, J. L., Canagaratna, M. R., Worsnop, D. R., Collins, D. R., Tomlinson, J., and Baltensperger, U.: Relating hygroscopicity and composition of organic aerosol particulate matter, Atmos. Chem. Phys., 11, 1155-1165, 10.5194/acp-11-1155-2011, 2011.

Ehn, M., Thornton, J. A., Kleist, E., Sipilä, M., Junninen, H., Pullinen, I., Springer, M., Rubach, F., Tillmann, R., Lee, B., Lopez-Hilfiker, F., Andres, S., Acir, I.-H., Rissanen, M., Jokinen, T., Schobesberger, S., Kangasluoma, J., Kontkanen, J., Nieminen, T., Kurtén, T., Nielsen, L. B., Jørgensen, S., Kjaergaard, H. G., Canagaratna, M., Maso, M. D., Berndt, T., Petäjä, T., Wahner, A., Kerminen, V.-M., Kulmala, M., Worsnop, D. R., Wildt, J., and Mentel, T. F.: A large source of low-volatility secondary organic aerosol, Nature, 506, 476, 10.1038/nature13032, 2014.

El-Sayed, M. M. H., Ortiz-Montalvo, D. L., and Hennigan, C. J.: The effects of isoprene and NOx on secondary organic aerosols formed through reversible and irreversible uptake to aerosol water, Atmos. Chem. Phys., 18, 1171-1184, 10.5194/acp-18-1171-2018, 2018.

Emery, C., Tai, E., and Yarwood, G.: Enhanced meteorological modeling and performance evaluation for two texas episodes, Report to the Texas Natural Resources Conservation Commission, prepared by ENVIRON, International Corp., Novato, CA,, available at: http://www.tceq.state.tx.us/assets/public/implementation/air/am/contracts/reports/mm/EnhancedMetModelingAndPerformanceEvaluation.pdf, 2001.

EPA: U.S.: Guidance on the Use of Models and Other Analyses for Demonstrating Attainment of Air Quality Goals for Ozone, PM2:5, and Regional Haze, EPA-454/B-07-002, 2007.

Ervens, B., Turpin, B. J., and Weber, R. J.: Secondary organic aerosol formation in cloud droplets and aqueous particles (aqSOA): a review of laboratory, field and model studies, Atmos. Chem. Phys., 11, 11069-11102, 10.5194/acp-11-11069-2011, 2011.

Fredenslund, A., Jones, R. L., and Prausnitz, J. M.: Group-contribution estimation of activity coefficients in nonideal liquid mixtures, AIChE J., 21, 1086-1099, doi:10.1002/aic.690210607, 1975.

Fu, H., and Chen, J.: Formation, features and controlling strategies of severe haze-fog pollutions in China, Sci. Total Environ., 578, 121-138, https://doi.org/10.1016/j.scitotenv.2016.10.201, 2017.

Galloway, M. M., Chhabra, P. S., Chan, A. W. H., Surratt, J. D., Flagan, R. C., Seinfeld, J. H., and Keutsch, F. N.: Glyoxal uptake on ammonium sulphate seed aerosol: reaction products and reversibility of uptake under dark and irradiated conditions, Atmos. Chem. Phys., 9, 3331-3345, 10.5194/acp-9-3331-2009, 2009.

Gentner, D. R., Jathar, S. H., Gordon, T. D., Bahreini, R., Day, D. A., El Haddad, I., Hayes, P. L., Pieber, S. M., Platt, S. M., de Gouw, J., Goldstein, A. H., Harley, R. A., Jimenez, J. L., Prévôt, A. S. H., and Robinson, A. L.: Review of Urban Secondary Organic Aerosol Formation from Gasoline and Diesel Motor Vehicle Emissions, Environ. Sci. Technol.,, 51,

1074-1093, 10.1021/acs.est.6b04509, 2017.

Guo, H., Xu, L., Bougiatioti, A., Cerully, K. M., Capps, S. L., Hite Jr, J. R., Carlton, A. G., Lee, S. H., Bergin, M. H., Ng, N. L., Nenes, A., and Weber, R. J.: Fine-particle water and pH in the southeastern United States, Atmos. Chem. Phys., 15, 5211-5228, 10.5194/acp-15-5211-2015, 2015.

Hayes, P. L., Carlton, A. G., Baker, K. R., Ahmadov, R., Washenfelder, R. A., Alvarez, S., Rappenglück, B., Gilman, J. B., Kuster, W. C., de Gouw, J. A., Zotter, P., Prévôt, A. S. H., Szidat, S., Kleindienst, T. E., Offenberg, J. H., Ma, P. K., and Jimenez, J. L.: Modeling the formation and aging of secondary organic aerosols in Los Angeles during CalNex 2010, Atmos. Chem. Phys., 15, 5773-5801, 10.5194/acp-15-5773-2015, 2015.

He, Q., Zhang, M., and Huang, B.: Spatio-temporal variation and impact factors analysis of satellite-based aerosol optical depth over China from 2002 to 2015, Atmos. Environ., 129, 79-90, https://doi.org/10.1016/j.atmosenv.2016.01.002, 2016.

He, Q., Gu, Y., and Zhang, M.: Spatiotemporal patterns of aerosol optical depth throughout China from 2003 to 2016, Sci. Total Environ., 653, 23-35, https://doi.org/10.1016/j.scitotenv.2018.10.307, 2019.

Healy, R. M., Temime, B., Kuprovskyte, K., and Wenger, J. C.: Effect of Relative Humidity on Gas/Particle Partitioning and Aerosol Mass Yield in the Photooxidation of p-Xylene, Environ. Sci. Technol.,, 43, 1884-1889, 10.1021/es802404z, 2009.

Hodzic, A., Jimenez, J. L., Madronich, S., Canagaratna, M. R., DeCarlo, P. F., Kleinman, L., and Fast, J.: Modeling organic aerosols in a megacity: potential contribution of semi-volatile and intermediate volatility primary organic compounds to secondary organic aerosol formation, Atmos. Chem. Phys., 10, 5491-5514, 10.5194/acp-10-5491-2010, 2010.

Hu, J., Chen, J., Ying, Q., and Zhang, H.: One-year simulation of ozone and particulate matter in China using WRF/CMAQ modeling system, Atmos. Chem. Phys., 16, 10333-10350, 10.5194/acp-16-10333-2016, 2016.

Hu, J., Wang, P., Ying, Q., Zhang, H., Chen, J., Ge, X., Li, X., Jiang, J., Wang, S., Zhang, J., Zhao, Y., and Zhang, Y.: Modeling biogenic and anthropogenic secondary organic aerosol in China, Atmos. Chem. Phys., 17, 77-92, 10.5194/acp-17-77-2017, 2017.

Huang, R.-J., Zhang, Y., Bozzetti, C., Ho, K.-F., Cao, J.-J., Han, Y., Daellenbach, K. R., Slowik, J. G., Platt, S. M., Canonaco, F., Zotter, P., Wolf, R., Pieber, S. M., Bruns, E. A., Crippa, M., Ciarelli, G., Piazzalunga, A., Schwikowski, M., Abbaszade, G., Schnelle-Kreis, J., Zimmermann, R., An, Z., Szidat, S., Baltensperger, U., Haddad, I. E., and Prévôt, A. S. H.: High secondary aerosol contribution to particulate pollution during haze events in China, Nature, 514, 218, 10.1038/nature13774, 2014.

Iacono, M. J., Delamere, J. S., Mlawer, E. J., Shephard, M. W., Clough, S. A., and Collins, W. D.: Radiative forcing by long-lived greenhouse gases: Calculations with the AER radiative transfer models, J. Geophys. Res., 113, D13103, 10.1029/2008jd009944, 2008.

Jathar, S. H., Mahmud, A., Barsanti, K. C., Asher, W. E., Pankow, J. F., and Kleeman, M. J.: Water uptake by organic aerosol and its influence on gas/particle partitioning of secondary organic aerosol in the United States, Atmos. Environ., 129, 142-154,

https://doi.org/10.1016/j.atmosenv.2016.01.001, 2016.

Jiang, F., Liu, Q., Huang, X., Wang, T., Zhuang, B., and Xie, M.: Regional modeling of secondary organic aerosol over China using WRF/Chem, J. Aerosol Sci., 43, 57-73, https://doi.org/10.1016/j.jaerosci.2011.09.003, 2012.

Jimenez, J. L., Canagaratna, M. R., Donahue, N. M., Prevot, A. S. H., Zhang, Q., Kroll, J. H., DeCarlo, P. F., Allan, J. D., Coe, H., Ng, N. L., Aiken, A. C., Docherty, K. S., Ulbrich, I. M., Grieshop, A. P., Robinson, A. L., Duplissy, J., Smith, J. D., Wilson, K. R., Lanz, V. A., Hueglin, C., Sun, Y. L., Tian, J., Laaksonen, A., Raatikainen, T., Rautiainen, J., Vaattovaara, P., Ehn, M., Kulmala, M., Tomlinson, J. M., Collins, D. R., Cubison, M. J., Dunlea, J., Huffman, J. A., Onasch, T. B., Alfarra, M. R., Williams, P. I., Bower, K., Kondo, Y., Schneider, J., Drewnick, F., Borrmann, S., Weimer, S., Demerjian, K., Salcedo, D., Cottrell, L., Griffin, R., Takami, A., Miyoshi, T., Hatakeyama, S., Shimono, A., Sun, J. Y., Zhang, Y. M., Dzepina, K., Kimmel, J. R., Sueper, D., Jayne, J. T., Herndon, S. C., Trimborn, A. M., Williams, L. R., Wood, E. C., Middlebrook, A. M., Kolb, C. E., Baltensperger, U., and Worsnop, D. R.: Evolution of Organic Aerosols in the Atmosphere, Science, 326, 1525-1529, 10.1126/science.1180353, 2009.

Kim, Y., Sartelet, K., and Couvidat, F.: Modeling the effect of non-ideality, dynamic mass transfer and viscosity on SOA formation in a 3-D air quality model, Atmos. Chem. Phys., 19, 1241-1261, 10.5194/acp-19-1241-2019, 2019.

Knote, C., Hodzic, A., Jimenez, J. L., Volkamer, R., Orlando, J. J., Baidar, S., Brioude, J., Fast, J., Gentner, D. R., Goldstein, A. H., Hayes, P. L., Knighton, W. B., Oetjen, H., Setyan, A., Stark, H., Thalman, R., Tyndall, G., Washenfelder, R., Waxman, E., and Zhang, Q.: Simulation of semi-explicit mechanisms of SOA formation from glyoxal in aerosol in a 3-D model, Atmos. Chem. Phys., 14, 6213-6239, 10.5194/acp-14-6213-2014, 2014.

Kurokawa, J., Ohara, T., Morikawa, T., Hanayama, S., Janssens-Maenhout, G., Fukui, T., Kawashima, K., and Akimoto, H.: Emissions of air pollutants and greenhouse gases over Asian regions during 2000–2008: Regional Emission inventory in ASia (REAS) version 2, Atmos. Chem. Phys., 13, 11019-11058, 10.5194/acp-13-11019-2013, 2013.

Lai, S., Zhao, Y., Ding, A., Zhang, Y., Song, T., Zheng, J., Ho, K. F., Lee, S.-c., and Zhong, L.: Characterization of PM2.5 and the major chemical components during a 1-year campaign in rural Guangzhou, Southern China, Atmospheric Research, 167, 208-215, https://doi.org/10.1016/j.atmosres.2015.08.007, 2016.

Lambe, A. T., Onasch, T. B., Massoli, P., Croasdale, D. R., Wright, J. P., Ahern, A. T., Williams, L. R., Worsnop, D. R., Brune, W. H., and Davidovits, P.: Laboratory studies of the chemical composition and cloud condensation nuclei (CCN) activity of secondary organic aerosol (SOA) and oxidized primary organic aerosol (OPOA), Atmos. Chem. Phys., 11, 8913-8928, 10.5194/acp-11-8913-2011, 2011.

Levy, R. C., Remer, L. A., Kleidman, R. G., Mattoo, S., Ichoku, C., Kahn, R., and Eck, T. F.: Global evaluation of the Collection 5 MODIS dark-target aerosol products over land, Atmos. Chem. Phys., 10, 10399-10420, 10.5194/acp-10-10399-2010, 2010.

Li, J., Cleveland, M., Ziemba, L. D., Griffin, R. J., Barsanti, K. C., Pankow, J. F., and Ying,

Q.: Modeling regional secondary organic aerosol using the Master Chemical Mechanism, Atmos. Environ., 102, 52-61, https://doi.org/10.1016/j.atmosenv.2014.11.054, 2015.

Li, J., Zhang, M., Wu, F., Sun, Y., and Tang, G.: Assessment of the impacts of aromatic VOC emissions and yields of SOA on SOA concentrations with the air quality model RAMS-CMAQ, Atmos. Environ., 158, 105-115, https://doi.org/10.1016/j.atmosenv.2017.03.035, 2017a.

Li, X., Song, S., Zhou, W., Hao, J., Worsnop, D. R., and Jiang, J.: Interactions between aerosol organic components and liquid water content during haze episodes in Beijing, Atmos. Chem. Phys., 19, 12163-12174, 10.5194/acp-19-12163-2019, 2019.

Li, Y. J., Sun, Y., Zhang, Q., Li, X., Li, M., Zhou, Z., and Chan, C. K.: Real-time chemical characterization of atmospheric particulate matter in China: A review, Atmos. Environ., 158, 270-304, https://doi.org/10.1016/j.atmosenv.2017.02.027, 2017b.

Lim, Y. B., Tan, Y., and Turpin, B. J.: Chemical insights, explicit chemistry, and yields of secondary organic aerosol from OH radical oxidation of methylglyoxal and glyoxal in the aqueous phase, Atmos. Chem. Phys., 13, 8651-8667, 10.5194/acp-13-8651-2013, 2013.

Lin, J., An, J., Qu, Y., Chen, Y., Li, Y., Tang, Y., Wang, F., and Xiang, W.: Local and distant source contributions to secondary organic aerosol in the Beijing urban area in summer, Atmos. Environ., 124, 176-185, https://doi.org/10.1016/j.atmosenv.2015.08.098, 2016.

Liu, J., Shen, J., Cheng, Z., Wang, P., Ying, Q., Zhao, Q., Zhang, Y., Zhao, Y., and Fu, Q.: Source apportionment and regional transport of anthropogenic secondary organic aerosol during winter pollution periods in the Yangtze River Delta, China, Sci. Total Environ., 710, 135620, https://doi.org/10.1016/j.scitotenv.2019.135620, 2020.

Liu, X.-H., Zhang, Y., Cheng, S.-H., Xing, J., Zhang, Q., Streets, D. G., Jang, C., Wang, W.-X., and Hao, J.-M.: Understanding of regional air pollution over China using CMAQ, part I performance evaluation and seasonal variation, Atmos. Environ., 44, 2415-2426, https://doi.org/10.1016/j.atmosenv.2010.03.035, 2010.

Luo, Y. X., Zheng, X. B., Zhao, T. L., and Chen, J.: A climatology of aerosol optical depth over China from recent 10 years of MODIS remote sensing data, Int. J. Climatol., 34, 863-870, 10.1002/joc.3728, 2014.

Malm, W. C., Sisler, J. F., Huffman, D., Eldred, R. A., and Cahill, T. A.: Spatial and seasonal trends in particle concentration and optical extinction in the United States, J. Geophys. Res., 99, 1347-1370, doi:10.1029/93JD02916, 1994.

Massoli, P., Lambe, A. T., Ahern, A. T., Williams, L. R., Ehn, M., Mikkilä, J., Canagaratna, M. R., Brune, W. H., Onasch, T. B., Jayne, J. T., Petäjä, T., Kulmala, M., Laaksonen, A., Kolb, C. E., Davidovits, P., and Worsnop, D. R.: Relationship between aerosol oxidation level and hygroscopic properties of laboratory generated secondary organic aerosol (SOA) particles, Geophys. Res. Lett., 37, 1-5, doi:10.1029/2010GL045258, 2010.

Murphy, B. N., Woody, M. C., Jimenez, J. L., Carlton, A. M. G., Hayes, P. L., Liu, S., Ng, N. L., Russell, L. M., Setyan, A., Xu, L., Young, J., Zaveri, R. A., Zhang, Q., and Pye, H. O. T.: Semivolatile POA and parameterized total combustion SOA in CMAQv5.2: impacts

on source strength and partitioning, Atmos. Chem. Phys., 17, 11107-11133, 10.5194/acp-17-11107-2017, 2017.

Odum, J. R., Hoffmann, T., Bowman, F., Collins, D., Flagan, R. C., and Seinfeld, J. H.: Gas/Particle Partitioning and Secondary Organic Aerosol Yields, Environ. Sci. Technol.,, 30, 2580-2585, 10.1021/es950943+, 1996.

Pankow, J. F.: An absorption model of gas/particle partitioning of organic compounds in the atmosphere, Atmos. Environ., 28, 185-188, https://doi.org/10.1016/1352-2310(94)90093-0, 1994.

Pankow, J. F., Marks, M. C., Barsanti, K. C., Mahmud, A., Asher, W. E., Li, J., Ying, Q., Jathar, S. H., and Kleeman, M. J.: Molecular view modeling of atmospheric organic particulate matter: Incorporating molecular structure and co-condensation of water, Atmos. Environ., 122, 400-408, https://doi.org/10.1016/j.atmosenv.2015.10.001, 2015.

Petters, M. D., and Kreidenweis, S. M.: A single parameter representation of hygroscopic growth and cloud condensation nucleus activity, Atmos. Chem. Phys., 7, 1961-1971, 10.5194/acp-7-1961-2007, 2007.

Prisle, N. L., Engelhart, G. J., Bilde, M., and Donahue, N. M.: Humidity influence on gas-particle phase partitioning of α-pinene + O3 secondary organic aerosol, Geophys. Res. Lett., 37, 1-5, 10.1029/2009gl041402, 2010.

Pye, H. O. T., Murphy, B. N., Xu, L., Ng, N. L., Carlton, A. G., Guo, H., Weber, R., Vasilakos, P., Appel, K. W., Budisulistiorini, S. H., Surratt, J. D., Nenes, A., Hu, W., Jimenez, J. L., Isaacman-VanWertz, G., Misztal, P. K., and Goldstein, A. H.: On the implications of aerosol liquid water and phase separation for organic aerosol mass, Atmos. Chem. Phys., 17, 343-369, 10.5194/acp-17-343-2017, 2017.

Qiao, X., Ying, Q., Li, X., Zhang, H., Hu, J., Tang, Y., and Chen, X.: Source apportionment of PM2.5 for 25 Chinese provincial capitals and municipalities using a source-oriented Community Multiscale Air Quality model, Sci. Total Environ., 612, 462-471, https://doi.org/10.1016/j.scitotenv.2017.08.272, 2018.

Ramanathan, V., Crutzen, P. J., Kiehl, J. T., and Rosenfeld, D.: Aerosols, Climate, and the Hydrological Cycle, Science, 294, 2119-2124, 10.1126/science.1064034, 2001.

Rickards, A. M. J., Miles, R. E. H., Davies, J. F., Marshall, F. H., and Reid, J. P.: Measurements of the Sensitivity of Aerosol Hygroscopicity and the κ Parameter to the O/C Ratio, J. Phys. Chem. A, 117, 14120-14131, 10.1021/jp407991n, 2013.

Robinson, A. L., Donahue, N. M., Shrivastava, M. K., Weitkamp, E. A., Sage, A. M., Grieshop, A. P., Lane, T. E., Pierce, J. R., and Pandis, S. N.: Rethinking Organic Aerosols: Semivolatile Emissions and Photochemical Aging, Science, 315, 1259-1262, 10.1126/science.1133061, 2007.

Seinfeld, J. H., Erdakos, G. B., Asher, W. E., and Pankow, J. F.: Modeling the Formation of Secondary Organic Aerosol (SOA). 2. The Predicted Effects of Relative Humidity on Aerosol Formation in the α-Pinene-, β-Pinene-, Sabinene-, Δ3-Carene-, and Cyclohexene-Ozone Systems, Environ. Sci. Technol.,, 35, 1806-1817, 10.1021/es001765+, 2001.

Shi, Z., Li, J., Huang, L., Wang, P., Wu, L., Ying, Q., Zhang, H., Lu, L., Liu, X., Liao, H.,

and Hu, J.: Source apportionment of fine particulate matter in China in 2013 using a source-oriented chemical transport model, Sci. Total Environ., 601-602, 1476-1487, https://doi.org/10.1016/j.scitotenv.2017.06.019, 2017.

Shrivastava, M., Cappa, C. D., Fan, J., Goldstein, A. H., Guenther, A. B., Jimenez, J. L., Kuang, C., Laskin, A., Martin, S. T., Ng, N. L., Petaja, T., Pierce, J. R., Rasch, P. J., Roldin, P., Seinfeld, J. H., Shilling, J., Smith, J. N., Thornton, J. A., Volkamer, R., Wang, J., Worsnop, D. R., Zaveri, R. A., Zelenyuk, A., and Zhang, Q.: Recent advances in understanding secondary organic aerosol: Implications for global climate forcing, Rev. Geophys., 55, 509-559, doi:10.1002/2016RG000540, 2017.

Shrivastava, M. K., Lane, T. E., Donahue, N. M., Pandis, S. N., and Robinson, A. L.: Effects of gas particle partitioning and aging of primary emissions on urban and regional organic aerosol concentrations, 113, 10.1029/2007jd009735, 2008.

Simon, H., and Bhave, P. V.: Simulating the Degree of Oxidation in Atmospheric Organic Particles, Environ. Sci. Technol.,, 46, 331-339, 10.1021/es202361w, 2012.

Sun, J., Liang, M., Shi, Z., Shen, F., Li, J., Huang, L., Ge, X., Chen, Q., Sun, Y., Zhang, Y., Chang, Y., Ji, D., Ying, Q., Zhang, H., Kota, S. H., and Hu, J.: Investigating the PM2.5 mass concentration growth processes during 2013–2016 in Beijing and Shanghai, Chemosphere, 221, 452-463, https://doi.org/10.1016/j.chemosphere.2018.12.200, 2019.

Sun, Y., Du, W., Fu, P., Wang, Q., Li, J., Ge, X., Zhang, Q., Zhu, C., Ren, L., Xu, W., Zhao, J., Han, T., Worsnop, D. R., and Wang, Z.: Primary and secondary aerosols in Beijing in winter: sources, variations and processes, Atmos. Chem. Phys., 16, 8309-8329, 10.5194/acp-16-8309-2016, 2016.

Sun, Y. L., Wang, Z. F., Fu, P. Q., Yang, T., Jiang, Q., Dong, H. B., Li, J., and Jia, J. J.: Aerosol composition, sources and processes during wintertime in Beijing, China, Atmos. Chem. Phys., 13, 4577-4592, 10.5194/acp-13-4577-2013, 2013.

Tkacik, D. S., Presto, A. A., Donahue, N. M., and Robinson, A. L.: Secondary Organic Aerosol Formation from Intermediate-Volatility Organic Compounds: Cyclic, Linear, and Branched Alkanes, Environ. Sci. Technol.,, 46, 8773-8781, 10.1021/es301112c, 2012.

Varutbangkul, V., Brechtel, F. J., Bahreini, R., Ng, N. L., Keywood, M. D., Kroll, J. H., Flagan, R. C., Seinfeld, J. H., Lee, A., and Goldstein, A. H.: Hygroscopicity of secondary organic aerosols formed by oxidation of cycloalkenes, monoterpenes, sesquiterpenes, and related compounds, Atmos. Chem. Phys., 6, 2367-2388, 10.5194/acp-6-2367-2006, 2006.

Wang, K., Zhang, Y., Jang, C., Phillips, S., and Wang, B.: Modeling intercontinental air pollution transport over the trans-Pacific region in 2001 using the Community Multiscale Air Quality modeling system, J. Geophys. Res., 114, D04307, doi:10.1029/2008JD010807, 2009.

Wiedensohler, A., Cheng, Y. F., Nowak, A., Wehner, B., Achtert, P., Berghof, M., Birmili, W., Wu, Z. J., Hu, M., Zhu, T., Takegawa, N., Kita, K., Kondo, Y., Lou, S. R., Hofzumahaus, A., Holland, F., Wahner, A., Gunthe, S. S., Rose, D., Su, H., and Pöschl, U.: Rapid aerosol particle growth and increase of cloud condensation nucleus activity by secondary aerosol formation and condensation: A case study for regional air pollution in

817 northeastern China, J. Geophys. Res., 114, D00G08, doi:10.1029/2008JD010884, 2009.

818 Wiedinmyer, C., Akagi, S. K., Yokelson, R. J., Emmons, L. K., Al-Saadi, J. A., Orlando,
819 J. J., and Soja, A. J.: The Fire INventory from NCAR (FINN): a high resolution global
820 model to estimate the emissions from open burning, Geosci. Model Dev., 4, 625-641,
821 10.5194/gmd-4-625-2011, 2011.

822 Woody, M. C., Baker, K. R., Hayes, P. L., Jimenez, J. L., Koo, B., and Pye, H. O. T.:
823 Understanding sources of organic aerosol during CalNex-2010 using the CMAQ-VBS,
824 Atmos. Chem. Phys., 16, 4081-4100, 10.5194/acp-16-4081-2016, 2016.

825 Ying, Q., Cureño, I. V., Chen, G., Ali, S., Zhang, H., Malloy, M., Bravo, H. A., and Sosa,
826 R.: Impacts of Stabilized Criegee Intermediates, surface uptake processes and higher
827 aromatic secondary organic aerosol yields on predicted PM2.5 concentrations in the
828 Mexico City Metropolitan Zone, Atmos. Environ., 94, 438-447,
829 https://doi.org/10.1016/j.atmosenv.2014.05.056, 2014.

830 Ying, Q., Li, J., and Kota, S. H.: Significant Contributions of Isoprene to Summertime
831 Secondary Organic Aerosol in Eastern United States, Environmental Science &
832 Technology, 49, 7834-7842, 10.1021/acs.est.5b02514, 2015.

833 Zhang, H., Hu, J., Kleeman, M., and Ying, Q.: Source apportionment of sulfate and nitrate
834 particulate matter in the Eastern United States and effectiveness of emission control
835 programs, Sci. Total Environ., 490, 171-181,
836 https://doi.org/10.1016/j.scitotenv.2014.04.064, 2014.

837 Zhang, Q., Streets, D. G., Carmichael, G. R., He, K. B., Huo, H., Kannari, A., Klimont, Z.,
838 Park, I. S., Reddy, S., Fu, J. S., Chen, D., Duan, L., Lei, Y., Wang, L. T., and Yao, Z. L.:
839 Asian emissions in 2006 for the NASA INTEX-B mission, Atmos. Chem. Phys., 9, 5131-
840 5153, 10.5194/acp-9-5131-2009, 2009.

841 Zhao, B., Wang, S., Donahue, N. M., Jathar, S. H., Huang, X., Wu, W., Hao, J., and
842 Robinson, A. L.: Quantifying the effect of organic aerosol aging and intermediate-volatility
843 emissions on regional-scale aerosol pollution in China, Sci. Rep., 6, 28815,
844 10.1038/srep28815, 2016a.

845 Zhao, D. F., Buchholz, A., Kortner, B., Schlag, P., Rubach, F., Fuchs, H., Kiendler-Scharr,
846 A., Tillmann, R., Wahner, A., Watne, Å. K., Hallquist, M., Flores, J. M., Rudich, Y.,
847 Kristensen, K., Hansen, A. M. K., Glasius, M., Kourtchev, I., Kalberer, M., and Mentel, T.
848 F.: Cloud condensation nuclei activity, droplet growth kinetics, and hygroscopicity of
849 biogenic and anthropogenic secondary organic aerosol (SOA), Atmos. Chem. Phys., 16,
850 1105-1121, 10.5194/acp-16-1105-2016, 2016b.

851 Zhao, J., Qiu, Y., Zhou, W., Xu, W., Wang, J., Zhang, Y., Li, L., Xie, C., Wang, Q., Du,
852 W., Worsnop, D. R., Canagaratna, M. R., Zhou, L., Ge, X., Fu, P., Li, J., Wang, Z.,
853 Donahue, N. M., and Sun, Y.: Organic Aerosol Processing During Winter Severe Haze
854 Episodes in Beijing, J. Geophys. Res., 124, 10248-10263, 10.1029/2019jd030832, 2019.

855 Zhao, Y., Hennigan, C. J., May, A. A., Tkacik, D. S., de Gouw, J. A., Gilman, J. B., Kuster,
856 W. C., Borbon, A., and Robinson, A. L.: Intermediate-Volatility Organic Compounds: A
857 Large Source of Secondary Organic Aerosol, Environ. Sci. Technol.,,, 48, 13743-13750,

858   10.1021/es5035188, 2014.

859   Zheng, B., Zhang, Q., Zhang, Y., He, K. B., Wang, K., Zheng, G. J., Duan, F. K., Ma, Y.

860   L., and Kimoto, T.: Heterogeneous chemistry: a mechanism missing in current models to

861   explain secondary inorganic aerosol formation during the January 2013 haze episode in

862   North China, Atmos. Chem. Phys., 15, 2031-2049, 10.5194/acp-15-2031-2015, 2015.

863

Table 1. Statistical analysis of modeled temperature (K) and relative humidity (%) of January and July of 2013 at the monitoring sites in different geographical areas as shown in Figure S1 and listed cities in Table S5.

		Northeast		NCP		Northwest		YRD		Central		SCB		PRD		Southwest		Benchmark
		Jan	Jul	Jan	Jul	Jan	Jul	Jan	Jul	Jan	Jul	Jan	Jul	Jan	Jul	Jan	Jul	
Temperature (K)	OBS	256.2	296.2	263.9	297.4	266.9	293.0	277.7	303.2	275.7	301.1	276.1	295.7	289.4	301.1	282.2	295.1	
	PRE	251.6	296.3	261.2	298.8	267.0	293.5	278.4	302.0	276.2	301.0	273.5	293.1	288.9	300.0	278.8	291.8	
	MB	-4.6	0.1	-2.7	1.4	0.1	0.5	0.7	-1.2	0.5	-0.1	-2.6	-2.6	-0.5	-1.0	-3.4	-3.4	$\leq\pm0.5$
	GE	5.5	1.8	4.0	2.3	3.6	3.2	2.0	2.3	2.6	2.4	5.1	4.2	1.9	1.8	4.1	3.5	≤2.0
	R	0.9	0.9	0.9	0.8	0.8	0.8	0.9	0.8	0.9	0.8	0.8	0.9	0.9	0.6	0.9	0.8	
Relative Humidity (%)	OBS	77.5	80.3	74.5	72.1	60.2	69.1	79.3	71.3	76.3	71.8	68.5	74.4	77.0	80.6	70.3	77.9	
	PRE	85.0	73.2	78.6	57.5	49.2	54.2	75.1	76.9	64.5	70.0	57.7	78.4	75.3	84.8	75.8	85.1	
	MB	7.5	-7.1	4.1	-14.6	-11.0	-15.0	-4.2	5.6	-11.8	-1.8	-10.8	4.0	-1.7	4.2	5.5	7.2	
	GE	11.3	11.3	14.6	16.6	19.8	19.1	11.0	11.6	16.8	11.7	22.8	11.6	9.5	9.2	15.4	10.4	
	R	0.5	0.8	0.4	0.8	0.3	0.7	0.6	0.6	0.6	0.6	0.2	0.6	0.6	0.5	0.5	0.7	

*OBS is mean observation, PRE is mean prediction, MB is mean bias, GE is gross error, R is the correlation coefficient of predictions vs. observations.

$MB=\sum_{i=1}^{N}(C_p - C_o)/N$; $GE=\sum_{i=1}^{N}|C_p - C_o|/N$, where C_p and C_o are the prediction and observation data, N is the total number of data.

**Northeast is Northeast China, NCP is North China Plain, Northwest is Northwest China, YRD is Yangtze River Delta, Central is Central China, SCB is Sichuan Basin, PRD is Pearl River Delta, Southwest is Southwest China.

***Benchmarks of MB and GE are for the MM5 model of 4-12 km horizontal resolution by Emery et al. (2001)
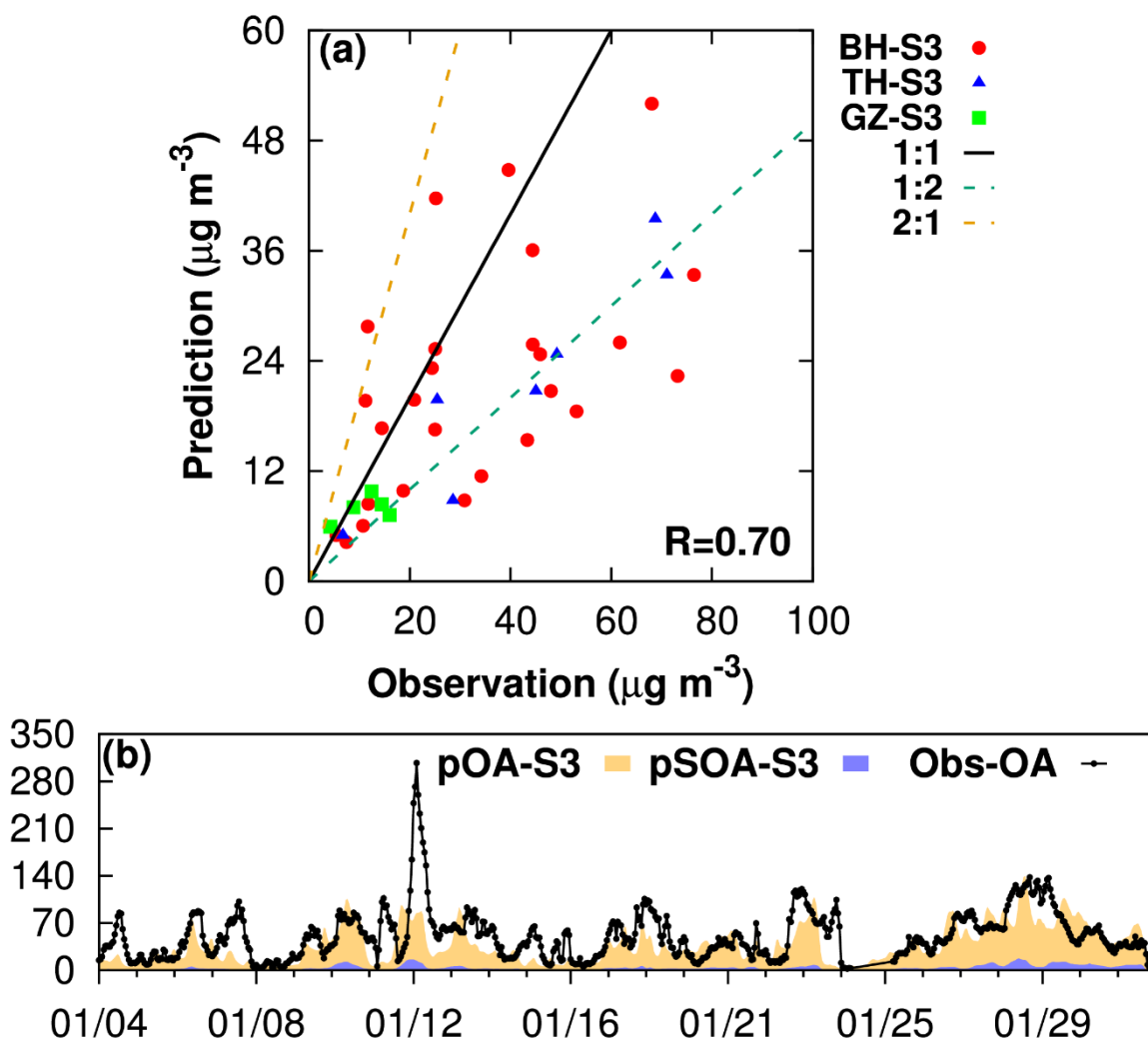
Figure 1. Comparison of (a) observed and modeled organic carbon concentration at University of Beihang (BH), Tsinghua University (TH) and Guangzhou (GZ); (b) observed organic aerosol (Obs-OA) at Beijing and predictions of total OA (pOA) and SOA (pSOA), unit is μg m^{-3}. Locations of monitoring sites are shown in Figure S1.
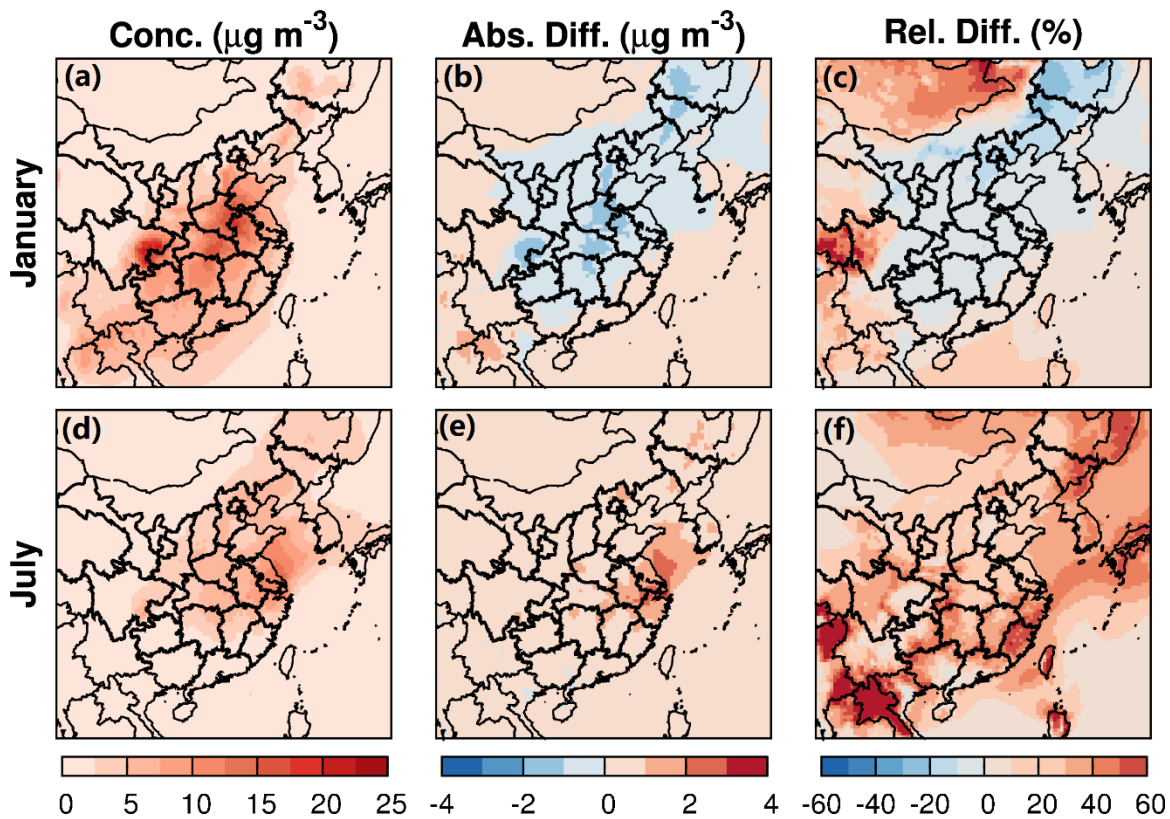
Figure 2. Monthly-averaged SOA from S3 and changes of SOA due to water partitioning into OPM and non-ideality of the organic-water mixture. "Abs. Diff." represents absolute differences (S3-BS); "Rel. Diff." represents relative differences ((S3-BS)/BS, %).
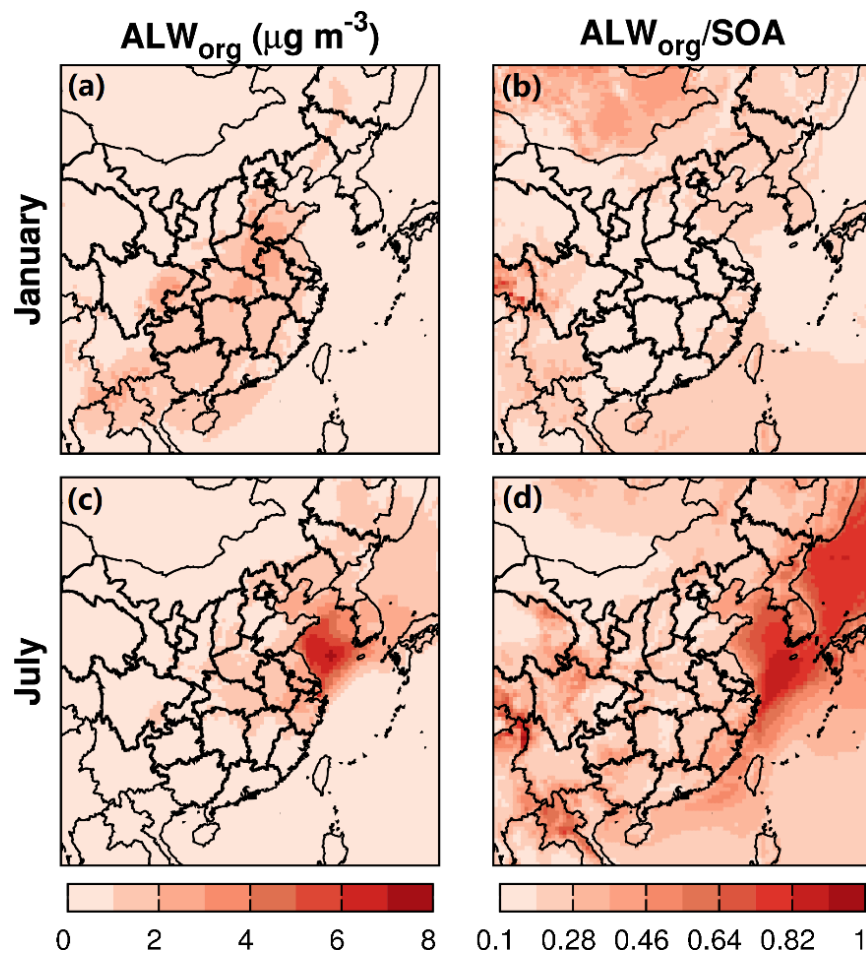
Figure 3. Monthly-averaged water partitioning into the organic-phase (ALW$_{org}$, μg m^{-3}) and the ratio to SOA (ALW$_{org}$/SOA) during January and July of 2013.
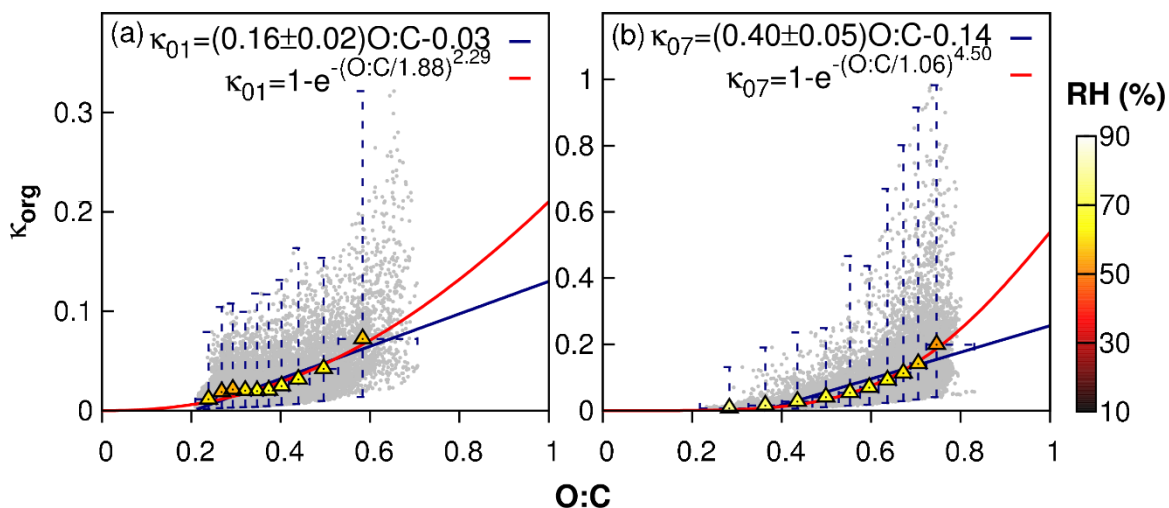
Figure 4. The correlation of hygroscopicity of organic aerosol (κ_{org}) and O:C ratio in 9 representative cities including Shenyang (SS), Beijing (BJ), Jinan (JN), Zhengzhou (ZZ), Xi'an (XA), Nanjing (NJ), Shanghai (SH), Chengdu (CD), and Guangzhou (GZ) in January (a) and July (b) of 2013. O:C ratios are categorized into 10 bins. In each bin, the ranges of O:C and κ_{org} are represented by bars. The mean values of O:C and κ_{org} are represented by triangles colored by the averaged RH of each bin. The relationship between κ_{org} and O:C is fitted by a linear function with reduced major axis regression (blue lines) and an exponential function (red lines), respectively. κ_{01} and κ_{07} represent the fitted correlation for January and July, respectively.
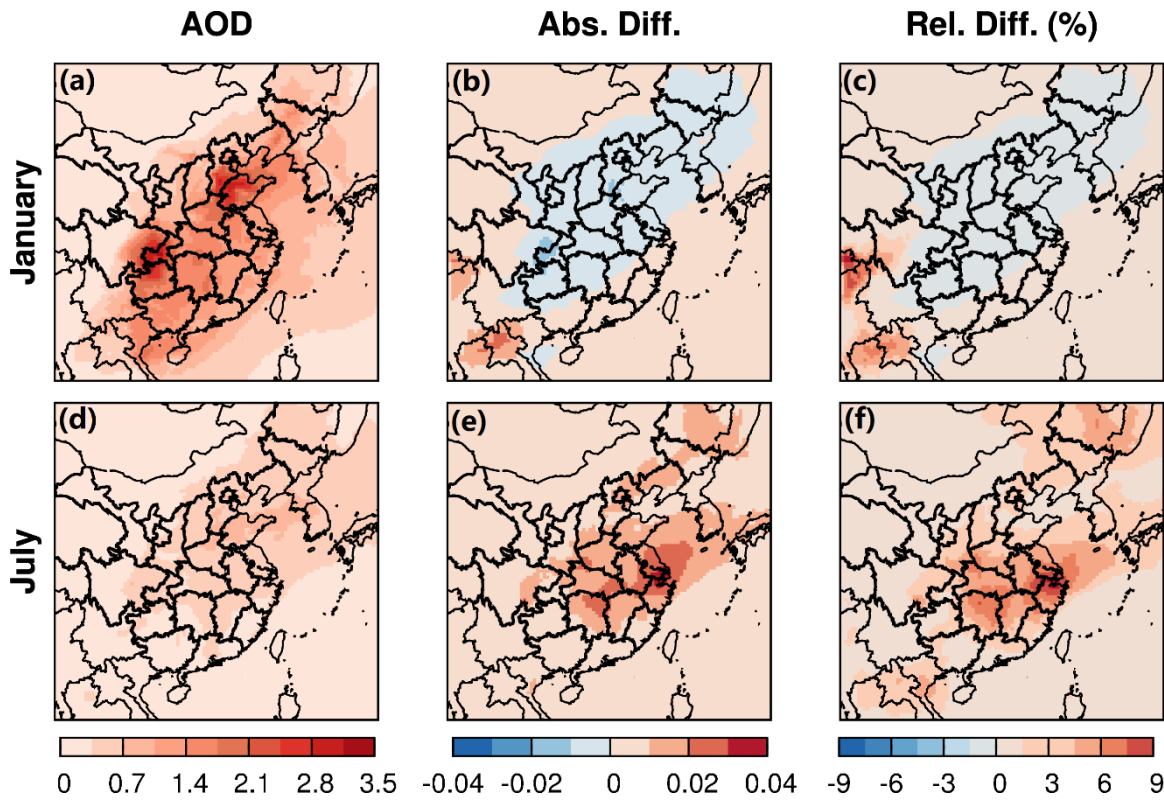
Figure 5. Monthly-averaged AOD_r at 550 nm and changes of AOD_r due to water partitioning into OPM and non-ideality of the organic-water mixture. "Abs. Diff." represents absolute differences (S3-BS); "Rel. Diff." represents relative differences ((S3-BS)/BS, %).
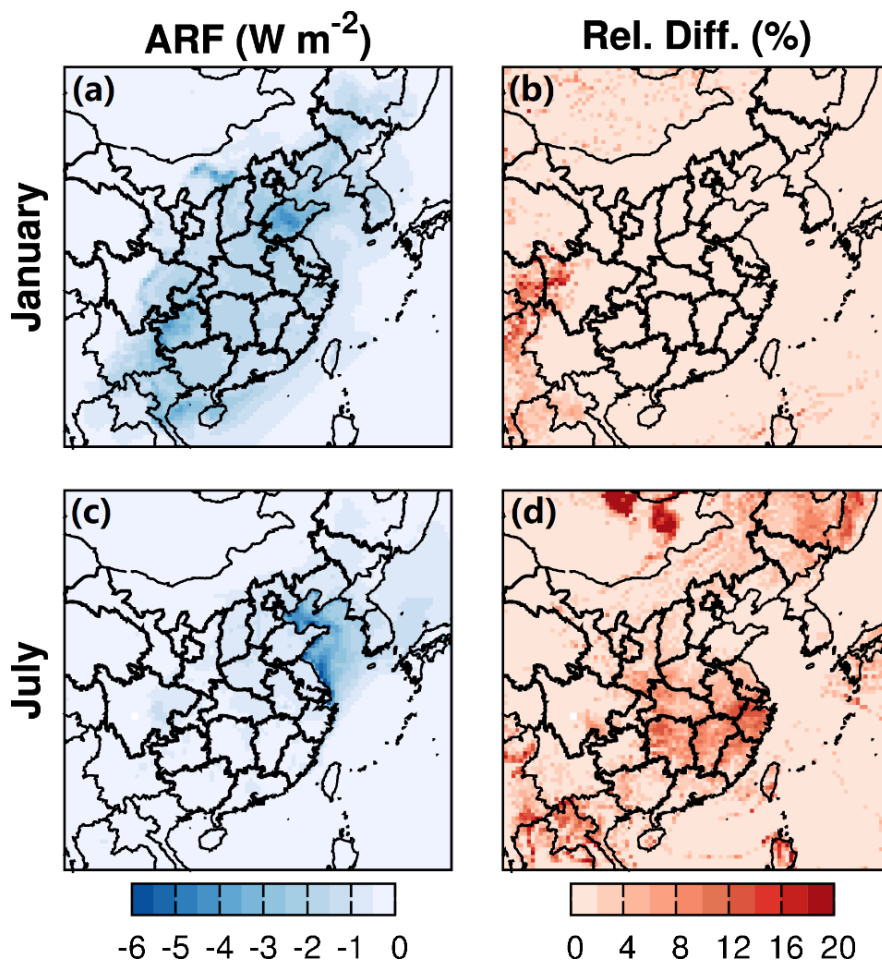
Figure 6. Monthly-averaged shortwave direct aerosol radiative forcing at the top of the atmosphere from S3 and the relative changes due to water partitioning into OPM and non-ideality of the organic-water mixture during January and July of 2013. "Rel. Diff." represents relative differences ((S3-BS)/BS, %).
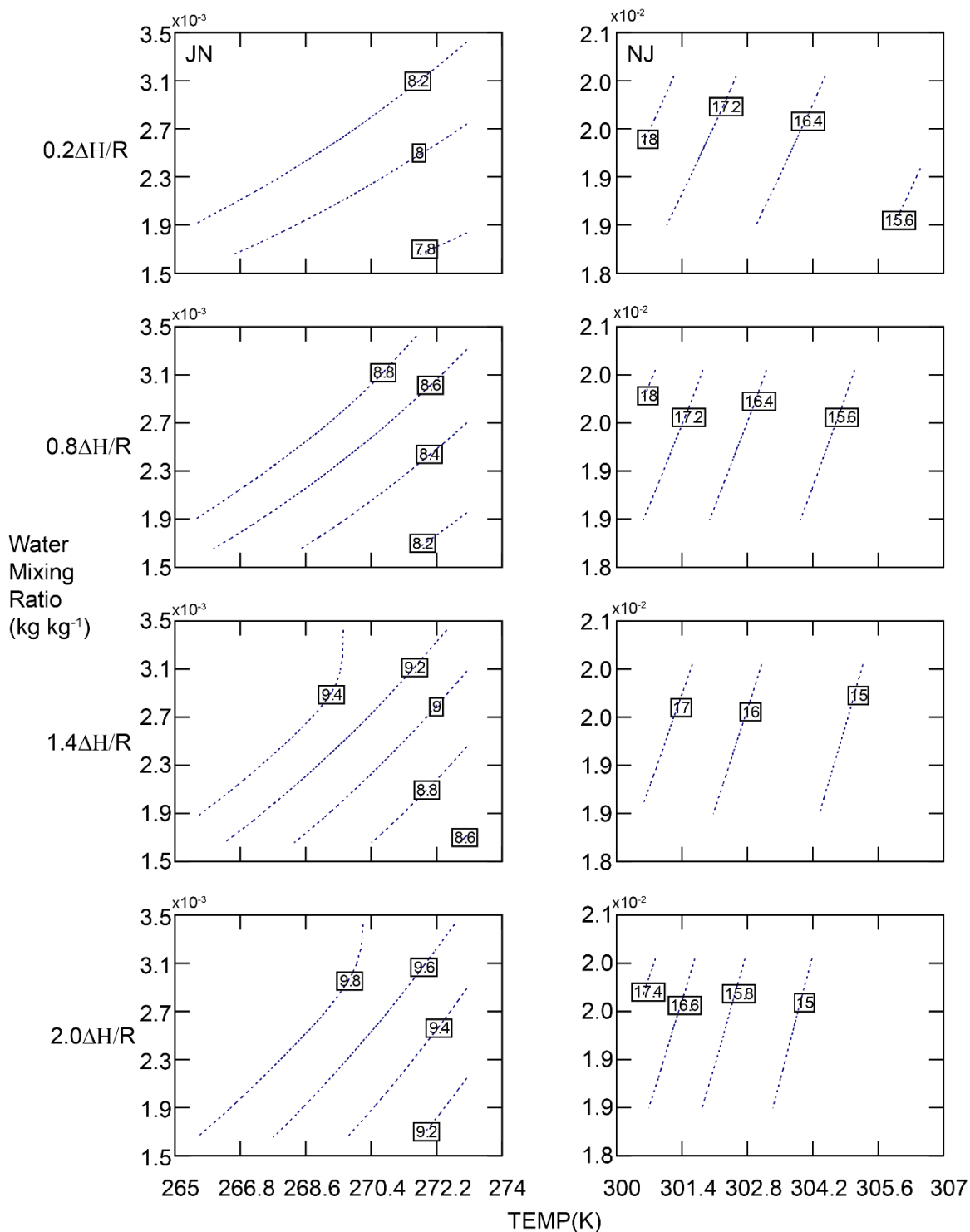
Figure 7. The sensitivity of SOA formation to temperature (TEMP), water mixing ratio, and the temperature dependence parameter of SVP ($\Delta H/R$) at Jinan (JN, first column) and Nanjing (NJ, second column).
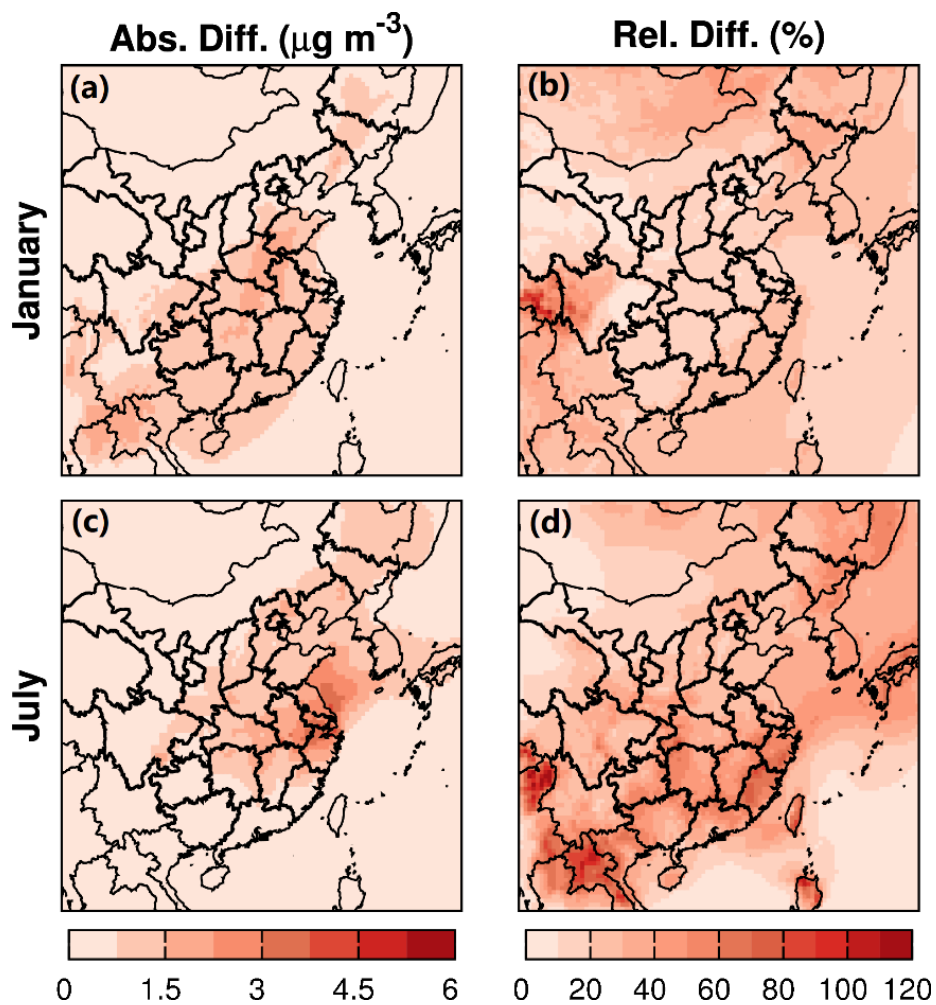
Figure 8. Monthly-averaged impacts of water partitioning into OPM on SOA. "Abs. Diff." represents absolute differences (S3-S2); "Rel. Diff." represents relative differences ((S3-S2)/S2, %).
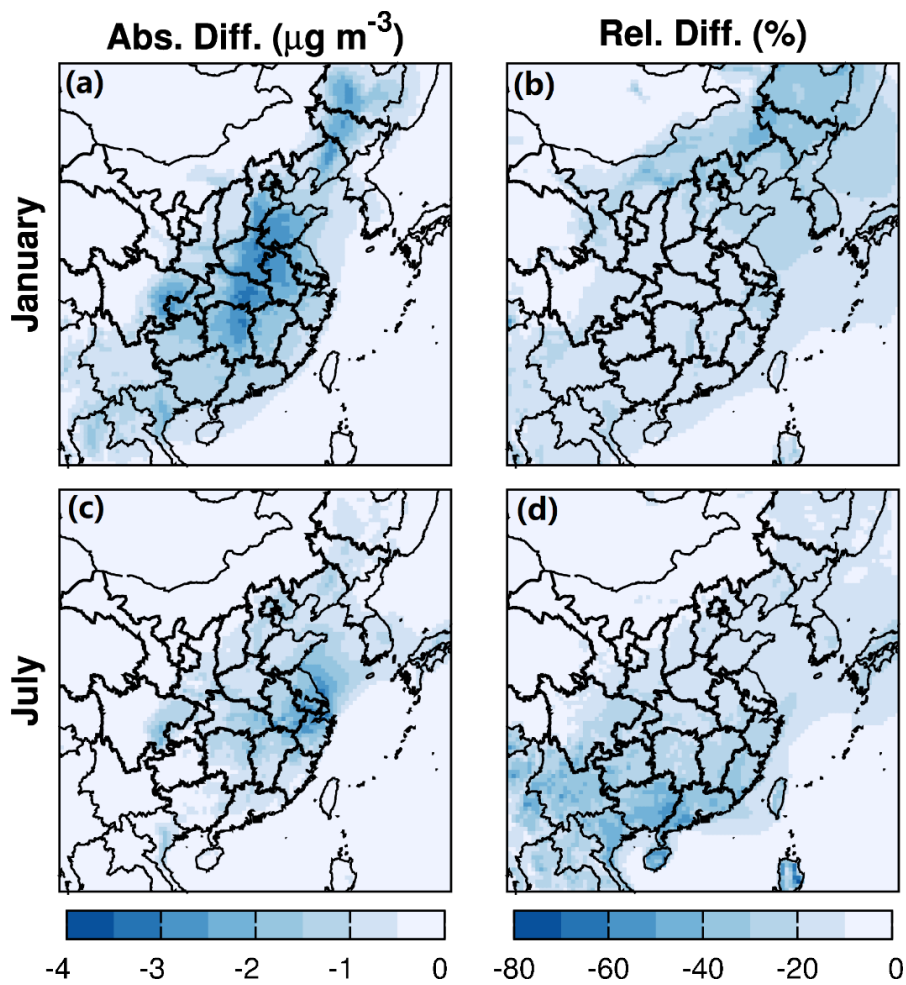
Figure 9. Monthly-averaged impacts of non-ideality of the organics-water mixture on SOA. "Abs. Diff." represents absolute differences (S3-S1); "Rel. Diff." represents relative differences ((S3-S1)/S1, %).